
Why Spectral Normalization Stabilizes GANs: Analysis and Improvements

Zinan Lin

Electrical and Computer Engineering
Carnegie Mellon University
Pittsburgh, PA 15213
zinanl@andrew.cmu.edu

Vyas Sekar

Electrical and Computer Engineering
Carnegie Mellon University
Pittsburgh, PA 15213
vsekar@andrew.cmu.edu

Giulia Fanti

Electrical and Computer Engineering
Carnegie Mellon University
Pittsburgh, PA 15213
gfanti@andrew.cmu.edu

Abstract

Spectral normalization (SN) is a widely-used technique for improving the stability of Generative Adversarial Networks (GANs) by forcing each layer of the discriminator to have unit spectral norm [25]. This approach controls the Lipschitz constant of the discriminator, and is empirically known to improve sample quality in many GAN architectures. However, there is currently little understanding of why SN is so effective. In this work, we show that SN controls two important failure modes of GAN training: exploding and vanishing gradients. Our proofs illustrate a (perhaps unintentional) connection with the successful LeCun initialization technique [20], proposed over two decades ago to control gradients in the training of deep neural networks. This connection helps to explain why the most popular implementation of SN for GANs [25] requires no hyperparameter tuning, whereas stricter implementations of SN have poor empirical performance out-of-the-box [12, 8]. Unlike LeCun initialization which only controls gradient vanishing at the beginning of training, we show that SN tends to preserve this property throughout training. Finally, building on this theoretical understanding, we propose Bidirectional Spectral Normalization (BSN), a modification of SN inspired by Xavier initialization [9], a later improvement to LeCun initialization. Theoretically, we show that BSN gives better gradient control than SN. Empirically, we demonstrate that BSN outperforms SN in sample quality on several benchmark datasets, while also exhibiting better training stability.

1 Introduction

Generative adversarial networks (GANs) are state-of-the-art deep generative models, perhaps best known for their ability to produce high-resolution, photorealistic images [11]. The objective of GANs is to produce random samples from a target data distribution, given only access to an initial set of training samples. This is achieved by learning two functions: a generator G , which maps random input noise to a generated sample, and a discriminator D , which tries to classify input samples as either real (i.e., from the training dataset) or fake (i.e., produced by the generator). In practice, these functions are implemented by deep neural networks (DNNs), and the competing generator and

discriminator are trained in an alternating process known as *adversarial training*. Theoretically, given enough data and model capacity, GANs converge to the true underlying data distribution [11].

Although GANs have been very successful in improving the sample quality of data-driven generative models [17, 5], their adversarial training also contributes to the well-studied instability of GANs. That is, small hyperparameter changes and even randomness in the optimization can cause training to fail. Many approaches have been proposed for improving the stability of GANs, including different architectures [32, 17, 5], loss functions [1, 2, 13, 41], and regularizations/normalizations [25, 6, 35]. One of the most successful proposals to date is called *spectral normalization* (SN) [25, 12, 8]. SN forces each layer of the generator to have unit spectral norm during training. This has the effect of controlling the Lipschitz constant of the discriminator, which is empirically observed to improve the stability of GAN training [25]. However, there are many ways to control the Lipschitz constant of a function. To date, it remains unclear precisely why this specific normalization is so effective.

In this paper, we show that SN controls two important failure modes of GAN training: exploding gradients and vanishing gradients. These problems are well-known to cause instability in GANs [2, 5], leading either to bad local minima or stalled training prior to convergence. SN mitigates both problems by tightly bounding the magnitudes of gradients. The fact that SN upper bounds gradient magnitudes may be expected, since SN was initially proposed to bound the discriminator’s Lipschitz constant. However, there is no reason *a priori* for SN to also mitigate the gradient vanishing problem.

Although our results and analysis are not unique to GANs, we focus on them because SN seems to have a disproportionately beneficial effect on GANs [25]. In this work, we make three primary contributions:

(1) *Analysis of why SN avoids exploding gradients.* Poorly-chosen architectures and hyperparameters, as well as randomness during training, can amplify the effects of large gradients on training instability, ultimately leading to generalization error in the learned discriminator. We show that SN imposes a strict upper bound on gradients during GAN training, mitigating these effects.

(2) *Analysis of why SN avoids vanishing gradients.* Small gradients during training are known to cause GANs (and other DNNs) to converge to bad models [20, 2]. The well-known LeCun initialization, first proposed over two decades ago, mitigates this effect by carefully choosing the variance of the initial weights [20]. We prove theoretically that SN controls the variance of weights in a way that closely parallels LeCun initialization, despite little connection between the two ideas at first glance. Whereas LeCun initialization only controls the gradient vanishing problem at the beginning of training, we show empirically that SN preserves this nice property throughout training. Our analysis also explains why a strict implementation of SN [8] has poor out-of-the-box performance on GANs and requires additional hyperparameter tuning to avoid the vanishing gradient problem, whereas the implementation of SN in [25] requires no hyperparameter tuning.

(3) *Improving SN with Bidirectional Spectral Normalization.* Based on our theoretical insights, we design an improved version of SN which we call *Bidirectional Spectral Normalization* (BSN). BSN is motivated by the so-called *Xavier initialization*, a refinement of LeCun initialization that controls not only the variances of internal outputs, but also the variance of backpropagated gradients [9]. We show that BSN achieves better or equal sample quality to SN on several benchmark datasets, including CIFAR10, STL10, CelebA, and ImageNet, while also exhibiting better stability during training.

2 Background and Preliminaries

The instability of GANs is believed to be predominantly caused by poor discriminator learning [1, 34]. We therefore focus in this work on the discriminator, and the effects of SN on discriminator learning. We adopt the same model as [25]. Consider a discriminator with L internal layers:

$$D_{\theta}(x) = a_L \circ l_{w_L} \circ a_{L-1} \circ l_{w_{L-1}} \circ \dots \circ a_1 \circ l_{w_1}(x) \quad (1)$$

where x denotes the input to the discriminator and $\theta = \{w_1, w_2, \dots, w_L\}$ the weights; a_i ($i = 1, \dots, L - 1$) is the activation function in the i -th layer, which is usually element-wise ReLU or leaky ReLU in GANs [11]. a_L is the activation function for the last layer, which is sigmoid for the vanilla GAN [11] and identity for WGAN-GP [13]; l_{w_i} is the linear transformation in i -th layer, which is usually fully-connected or a convolutional neural network [11, 32].

Lipschitz Regularization and Spectral Normalization. Prior work has shown that regularizing the Lipschitz constant of the discriminator $\|D_{\theta}\|_{\text{Lip}}$ improves the stability of GANs [2, 13, 41]. For

example, WGAN-GP [13] adds a gradient penalty $(\|\nabla D_\theta(\tilde{x})\| - 1)^2$ to the loss function, where $\tilde{x} = \alpha x + (1 - \alpha)G(z)$ and $\alpha \sim \text{Uniform}(0, 1)$ to ensure that the Lipschitz constant of the discriminator is bounded by 1.

Spectral normalization (SN) takes a different approach. For fully connected layers (i.e. $l_{w_i}(x) = w_i x$), it regularizes the weights w_i to ensure that spectral norm $\|w_i\|_{\text{sp}} = 1$ for all $i \in [1, L]$, where the spectral norm $\|w_i\|_{\text{sp}}$ is defined as the largest singular value of w_i . This bounds the Lipschitz constant of the discriminator since $\|D_\theta\|_{\text{Lip}} \leq \prod_{i=1}^L \|l_{w_i}\|_{\text{Lip}} \cdot \prod_{i=1}^L \|a_i\|_{\text{Lip}} \leq \prod_{i=1}^L \|w_i\|_{\text{sp}} \cdot \prod_{i=1}^L \|a_i\|_{\text{Lip}} \leq 1$, as $\|l_{w_i}\|_{\text{Lip}} \leq \|w_i\|_{\text{sp}}$ and $\|a_i\|_{\text{Lip}} \leq 1$ for networks with (leaky) ReLU as activation functions for the internal layers and identity/sigmoid as the activation function for the last layer [25]. Prior work has theoretically connected the generalization gap of neural networks to the product of the spectral norms of the layers [3, 27]. These insights led to multiple implementations of spectral normalization [8, 12, 42, 25], with the implementation of [25] achieving particular success on GANs. SN can be viewed as a special case of more general techniques for enhancing stability of neural network training by controlling the spectrum of the network’s input-output Jacobian [31], e.g., through techniques like Jacobian clamping [28], which constrains the values of the maximum and minimum singular values in the generator during training.

In practice, spectral normalization [8, 25] is implemented by dividing the weight matrix w_i by its spectral norm: $\frac{w_i}{u_i^T w_i v_i}$, where u_i and v_i are the left/right singular vectors of w_i corresponding to its largest singular value. As observed by Gouk et al. [12], there are two approaches in the SN literature for instantiating the matrix w_i for convolutional neural networks (CNNs). In a CNN, since convolution is a linear operation, convolutional layers can equivalently be written as a multiplication by an expanded weight matrix \tilde{w}_i that is derived from the raw weights w_i . Hence in principle, spectral normalization should normalize each convolutional layer by $\|\tilde{w}_i\|_{\text{sp}}$ [12, 8]. We call this canonical normalization SN_{Conv} as it controls the spectral norm of the convolution layer.

However, the spectral normalization that is known to outperform other regularization techniques and improve training stability for GANs [25], which we call SN_w , does not implement SN in a strict sense. Instead, it uses $\|w_i^{c_{\text{out}} \times (c_{\text{in}} k_w k_h)}\|_{\text{sp}}$; that is, it first reshapes the convolution kernel $w_i \in \mathbb{R}^{c_{\text{out}} c_{\text{in}} k_w k_h}$ into a matrix \hat{w}_i of shape $c_{\text{out}} \times (c_{\text{in}} k_w k_h)$, and then normalizes with the spectral norm $\|\hat{w}_i\|_{\text{sp}}$, where c_{in} is the number of input channels, c_{out} is the number of output channels, k_w is the kernel width, and k_h is the kernel height. Miyato et al. showed that their implementation implicitly penalizes w_i from being too sensitive in one specific direction [25]. However, this does not explain why SN_w is more stable than other Lipschitz regularization techniques, and as observed in [12], it is unclear how SN_w relates to SN_{Conv} . Despite this, SN_w has empirically been immensely successful in stabilizing the training of GANs [5, 23, 44, 16, 43, 26, 22]. Even more puzzling, we show in § 4 that the canonical approach SN_{Conv} has comparatively poor out-of-the-box performance when training GANs.

Hence, two questions arise: (1) Why is SN so successful at stabilizing the training of GANs? (2) Why is SN_w proposed by [25] so much more effective than the canonical SN_{Conv} ?

Gradient explosion and vanishing. In this work, we show that both questions are related to two well-known phenomena: vanishing and exploding gradients. These terms describe a problem in which gradients either grow or shrink rapidly during training [4, 29, 30], and they are known to be closely related to the instability of GANs [1, 5]. We provide an example to illustrate how vanishing or exploding gradients cause training instability in GANs in App. I.

3 Exploding Gradients

In this section, we show that spectral normalization prevents gradient explosion by bounding the gradients of the discriminator. Moreover, we show that the common choice to normalize all layers equally achieves the tightest upper bound for a restricted class of discriminators. We use $\theta \in \mathbb{R}^d$ to denote a vector containing all elements in $\{w_1, \dots, w_L\}$. In the following analysis, we assume linear transformations are fully-connected layers $l_{w_i}(x) = w_i x$ as in [25], though the same analysis can be applied to convolutional layers.

To highlight the effects of the spectral norm of each layer on the gradient and simplify the exposition, we will compute gradients with respect to $w'_i = \frac{w_i}{w_i^T w_i v_i}$ in the following discussion. In reality, gradients are computed with respect to w_i ; we defer this discussion to App. C, where we show the relevant extension. The following proposition shows that under this simplifying assumption, spectral normalization controls the magnitudes of the gradients of the discriminator with respect to θ . Notice that simply controlling the Lipschitz constant of the discriminator (e.g., as in WGAN [1]) does not imply this property; it instead ensures small (sub)gradients with respect to the input, x .

Proposition 1 (Upper bound of gradient’s Frobenius norm for spectral normalization). *If $\|w_i\|_{sp} \leq 1$ for all $i \in [1, L]$, then we have $\|\nabla_{w_t} D_\theta(x)\|_F \leq \|x\| \prod_{i=1}^L \|a_i\|_{Lip}$, and the norm of the overall gradient can be bounded by $\|\nabla_\theta D_\theta(x)\|_F \leq \sqrt{L} \|x\| \prod_{i=1}^L \|a_i\|_{Lip}$.*

(Proof in App. A). Note that under the assumption that internal activation functions are ReLU or leaky ReLU, if the activation function for the last layer is identity (e.g., for WGAN-GP [13]), the above bounds can be simplified to $\|\nabla_{w_t} D_\theta(x)\|_F \leq \|x\|$ and $\|\nabla_\theta D_\theta(x)\| \leq \sqrt{L} \|x\|$, and if the activation for the last layer is sigmoid (e.g., for vanilla GAN [11]), the above bounds become $\|\nabla_{w_t} D_\theta(x)\|_F \leq 0.25 \|x\|$ and $\|\nabla_\theta D_\theta(x)\| \leq 0.25 \sqrt{L} \|x\|$. A comparable bound can also be found to limit the norm of the Hessian, which we defer to App. D due to space constraints.

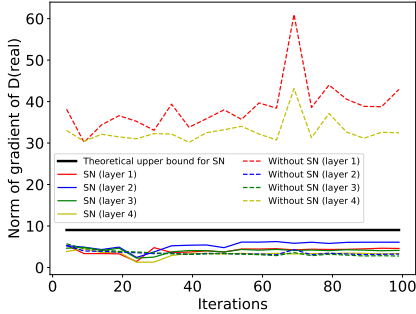


Figure 1: Gradient norms of each discriminator layer in MNIST.

the product of the spectral norm bounds is the same.

Proposition 2. *For any discriminator $D_\theta = a_L \circ l_{w_L} \circ a_{L-1} \circ l_{w_{L-1}} \circ \dots \circ a_1 \circ l_{w_1}$ and $D'_\theta = a_L \circ l_{c_L \cdot w_L} \circ a_{L-1} \circ l_{c_{L-1} \cdot w_{L-1}} \circ \dots \circ a_1 \circ l_{c_1 \cdot w_1}$ where the internal activation functions $\{a_i\}_{i=1}^{L-1}$ are ReLU or leaky ReLU, and positive constant scalars c_1, \dots, c_L satisfy that $\prod_{i=1}^L c_i = 1$, we have*

$$D_\theta(x) = D'_\theta(x) \quad \forall x \quad \text{and} \quad \frac{\partial^n D_\theta(x)}{\partial x^n} = \frac{\partial^n D'_\theta(x)}{\partial x^n} \quad \forall x, \forall n \in \mathbb{Z}^+. \quad (2)$$

(Proof in App. B). Given this observation, it is natural to ask if there is any benefit to setting the spectral norms of each layer equal. It turns out that the answer is yes, under some assumptions that appear to approximately hold in practice. Let

$$\mathcal{D} \triangleq \left\{ D_\theta = a_L \circ l_{w_L} \circ \dots \circ a_1 \circ l_{w_1} : \frac{\|\nabla_{w_i} D_\theta(x)\|_F}{\|\nabla_{w_j} D_\theta(x)\|_F} = \frac{\|w_j\|_{sp}}{\|w_i\|_{sp}}, a_i \in \{\text{ReLU, leaky ReLU}\} \forall i, j \in [1, L] \right\}. \quad (3)$$

This intuitively describes the set of all discriminators for which scaling up the weight of one layer proportionally increases the gradient norm of all other layers; the definition of this set is motivated by our upper bound on the gradient norm (App. A). The following theorem shows that when optimizing over set \mathcal{D} , choosing every layer to have the same spectral norm gives the smallest possible gradient norm, for a given set of parameters.

Theorem 1. *Consider a given set of discriminator parameters $\theta = \{w_1, \dots, w_L\}$. For a vector $c = \{c_1, \dots, c_L\}$, we denote $\theta_c \triangleq \{c_t w_t\}_{t=1}^L$. Let $\lambda_\theta = \prod_{i=1}^L \|w_i\|_{sp}^{1/L}$ denote the geometric mean of the spectral norms of the weights. Then we have*

$$\left\{ \frac{\lambda_\theta}{\|w_1\|_{sp}}, \dots, \frac{\lambda_\theta}{\|w_L\|_{sp}} \right\} = \arg \min_{c: D_{\theta_c} \in \mathcal{D}, \prod_{i=1}^L c_i = 1, c_i \in \mathbb{R}^+} \|\nabla_{\theta_c} D_{\theta_c}(x)\|_F \quad (4)$$

The bound in Prop. 1 has a significant effect in practice. Fig. 1 shows the norm of the gradient for each layer of a WGAN trained on MNIST with and without spectral normalization. Without spectral normalization, some layers have extremely large gradients throughout training, which makes the overall gradient large. With spectral normalization, the gradients of all layers are upper bounded as shown in Prop. 1. We see similar results in other datasets and network architectures (App. J).

Optimal Spectral Norm Allocation Common implementations of SN advocate setting the spectral norm of each layer to the same value [25, 8]. However, the following proposition states that we can set the spectral norms of different layers to different constants, without changing the network’s behavior on the input samples, as long as

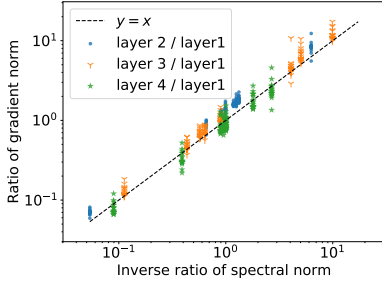


Figure 2: Ratio of gradient norm v.s. ratio of spectral norm in MNIST.

of points are from different epochs of the same run, therefore their ratio of spectral norms is the same. The fact that most of the points are near the diagonal line suggests that training naturally favors discriminators that are in or near \mathcal{D} ; we confirm this intuition in other experimental settings in App. K. This observation, combined with Thm. 1, suggests that it is better to force the spectral norms of every layer to be equal. Hence, existing SN implementations [25, 8] chose the correct, uniform normalization across layers to upper bound discriminator’s gradients.

(*Proof in App. E*). The key constraint in this theorem is that we optimize only over discriminators in set \mathcal{D} Eq. (3). To show that this constraint is realistic (i.e. SN GAN discriminator optimization tends to choose models in \mathcal{D}), we trained a spectrally-normalized GAN with four hidden layers on MNIST, computing the ratios of the gradient norms at each layer and the ratios of the spectral norms, as dictated by Eq. (3). We computed these ratios at different epochs during training, as well as for different randomly-selected rescalings of the spectral normalization vector c . Each point in Fig. 2 represents the results averaged over 64 real samples at a specific epoch of training for a given (random) c . Vertical series

4 Vanishing Gradients

An equally troublesome failure mode of GAN training is vanishing gradients [1]. Prior work has proposed new objective functions to mitigate this problem [1, 2, 13], but these approaches do not fully solve the problem (see Fig. 11). In this section, we show that SN also controls gradient vanishing.

Gradients tend to vanish for two reasons. First, gradients vanish when the objective function *saturates* [20, 1], which is often associated with function parameters growing too large. Common loss functions (e.g., hinge loss) and activation functions (e.g., sigmoid, tanh) saturate for inputs of large magnitude. Large parameters tend to amplify the inputs to the activation functions and/or loss function, causing saturation. Second, gradients vanish when function parameters (and hence, internal outputs) grow too small. This is because backpropagated gradients are scaled by the function parameters (App. A)

These insights motivated the LeCun initialization technique [20]. The key idea is that to prevent gradients from vanishing, we must ensure that the outputs of each neuron do not vanish or explode. If the inputs to a neural unit are uncorrelated random variables with variance 1, then to ensure that the unit’s output also has variance (approximately) 1, the weight parameters should be zero-mean random variables with variance of one over the fan-in to the node (number of incoming connections) [20]. Hence, LeCun initialization prevents gradient vanishing by controlling the variance of the individual parameters. In the following theorem, we show that SN enforces a similar condition.

Theorem 2 (Variance of spectrally-normalized weights). *For a matrix $A \in \mathbb{R}^{m \times n}$ with i.i.d entries a_{ij} from a symmetric distribution (e.g. zero-mean Gaussian or uniform), we have*

$$\text{Var} \left(\frac{a_{ij}}{\|A\|_{sp}} \right) \leq \frac{1}{\max\{m, n\}} . \quad (5)$$

Furthermore, if $m, n \geq 2$ and $\max\{m, n\} \geq 3$, and a_{ij} are from a zero-mean Gaussian, we have

$$\frac{L}{\max\{m, n\} \log(\min\{m, n\})} \leq \text{Var} \left(\frac{a_{ij}}{\|A\|_{sp}} \right) \leq \frac{1}{\max\{m, n\}} ,$$

where L is a constant which does not depend on m, n .

(*Proof in App. F*). In other words, spectral normalization forces zero-mean parameters to have a variance that scales inversely with $\max\{m, n\}$. The proof relies on a characterization of extreme values of random vectors drawn uniformly from the surface of a high-dimensional unit ball. Notice that this result holds regardless of the variance of the initial entries of A , suggesting that *SN is insensitive to initialization parameters*. Many fully-connected, feed-forward neural networks have a fixed width across hidden layers, so $\max\{m, n\}$ corresponds precisely to the fan-in of any neuron in a hidden layer, implying that SN has an effect like LeCun initialization.

In a CNN, the interpretation of $\max\{m, n\}$ depends on how SN is implemented. Recall that the implementation SN_w by Miyato et al. [25] does not strictly implement SN, but a variant that normalizes by the spectral norm of $\hat{w}_i = w_i^{c_{out} \times (c_{in} k_w k_h)}$. In architectures like DCGAN [32], the larger dimension of \hat{w}_i for *hidden layers* tends to be $c_{in} k_w k_h$, which corresponds to the fan-in. This means that SN gets the right variance for hidden layers in CNN. Our theoretical analysis only applies at initialization, when the parameters are selected randomly. However, unlike LeCun initialization which only controls the variance at initialization, we find empirically that Eq. (5) for SN appears to hold *throughout training* (Fig. 3). As a comparison, if trained without SN, the variance increases and the gradient decreases, which makes sample quality bad (App. L.2). This explains why in practice GANs trained with SN are stable *throughout training*.

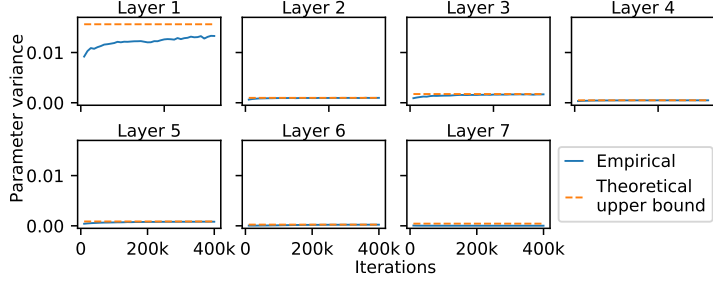


Figure 3: Parameter variances throughout training in CIFAR10.

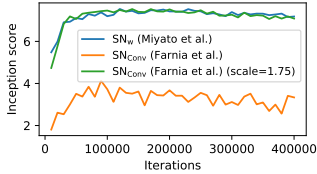


Figure 4: Inception score of different SN variants in CIFAR10.

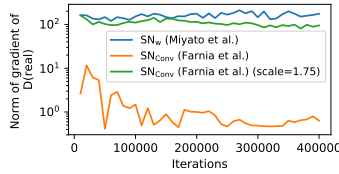


Figure 5: Gradient norms of different SN variants in CIFAR10.

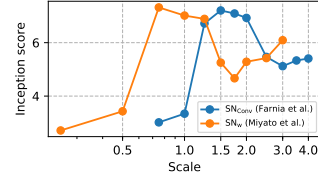


Figure 6: Inception score of scaled SN in CIFAR10.

Perhaps surprisingly, we find empirically that the strict implementation SN_{Conv} of [8] does *not* prevent gradient vanishing. Figs. 4 and 5 shows the gradients of SN_{Conv} vanishing when trained on CIFAR10, leading to a comparatively poor inception score, whereas the gradients of SN_w remain stable. To understand this phenomenon, recall that SN_{Conv} normalizes by the spectral norm of an expanded matrix \tilde{w}_i derived from w_i . Thm. 2 does not hold for \tilde{w}_i since its entries are not i.i.d. (even at initialization); hence it cannot be used to explain this effect. However, Corollary 1 in [38] shows that $\|\hat{w}_i\|_{\text{sp}} \leq \|\tilde{w}_i\|_{\text{sp}} \leq \alpha \|w_i\|_{\text{sp}}$, where α is a constant only depends on kernel size, input size, and stride size of the convolution operation. This result has two implications:

- (1) $\|\hat{w}_i\|_{\text{sp}} \leq \alpha \|w_i\|_{\text{sp}}$: Although SN_w does not strictly normalize the matrix with the actual spectral norm of the layer, it does upper bound the spectral norm of the layer. Therefore, all our analysis in § 3 still applies for SN_w by changing the spectral norm constant from 1 to $\alpha \|w_i\|_{\text{sp}}$. This means that SN_w can still prevent gradient explosion.
- (2) $\|\hat{w}_i\|_{\text{sp}} \leq \|\tilde{w}_i\|_{\text{sp}}$: This implies that SN_{Conv} normalizes by a factor that is at least as large as SN_w . In fact, we observe empirically that $\|\tilde{w}_i\|_{\text{sp}}$ is strictly larger than $\|w_i\|_{\text{sp}}$ during training (App. L.3). This means that for the same w_i , a discriminator using SN_{Conv} will have smaller outputs than the discriminator using SN_w . We hypothesize that the different scalings explain why SN_{Conv} has vanishing gradients but SN_w does not.

To confirm this hypothesis, for SN_w and SN_{Conv} , we propose to multiply all the normalized weights by a scaling factor s , which is fixed throughout the training. Fig. 6 shows that SN_{Conv} seems to be a shifted version of SN_w . SN_{Conv} with $s = 1.75$ has similar inception score (Fig. 4) to SN_w , as well as similar gradients (Fig. 5) and parameter variances (App. L.4) throughout training. This, combined with Thm. 2, suggests that SN_w inherently finds the correct scaling for the problem, whereas “proper” spectral normalization SN_{Conv} requires additional hyperparameter tuning.

5 Bidirectional Spectral Normalization: Improving Spectral Normalization

In 2010, Glorot and Bengio [9] built on the intuition of LeCun [20] to design an improved initialization, commonly called *Xavier initialization*. Their key observation was that to limit gradient vanishing (and explosion), it is not enough to control only feed-forward outputs; we should also control the variance of backpropagated gradients. Let n_i, m_i denote the fan-in and fan-out of layer i . (In fully-connected layers, $n_i = m_{i-1}$ = the width of layer i .) Whereas LeCun chooses initial parameters with variance $\frac{1}{n_i}$, Glorot and Bengio choose them with variance $\frac{2}{n_i+m_i}$, a compromise between $\frac{1}{n_i}$ (to control output variance) and $\frac{1}{m_i}$ (to control variance of backpropagated gradients).

We propose Bidirectional Spectral Normalization (BSN), which applies a similar intuition to improve the spectral normalization of Miyato *et al.* [25]. For fully connected layers, we keep the normalization the same as SN_w [25]. For convolution layers, instead of normalizing by $\|w^{c_{out} \times (c_{in} k_w k_h)}\|_{sp}$, we normalize by $\sigma_w \triangleq \frac{\|w^{c_{out} \times (c_{in} k_w k_h)}\|_{sp} + \|w^{c_{in} \times (c_{out} k_w k_h)}\|_{sp}}{2}$, where $\|w^{c_{in} \times (c_{out} k_w k_h)}\|_{sp}$ is the spectral norm of the reshaped convolution kernel of dimension $c_{in} \times (c_{out} k_w k_h)$. For calculating these two spectral norms, we use the same power iteration method in [25]. The following theorem gives the theoretical explanation.

Theorem 3 (Variance of Bidirectional Spectral Normalization). *For a convolutional kernel $w \in \mathbb{R}^{c_{out} c_{in} k_w k_h}$ with i.i.d. entries w_{ij} from a symmetric distribution (e.g. zero-mean Gaussian or uniform) where $k_w k_h \geq \max\left\{\frac{c_{out}}{c_{in}}, \frac{c_{in}}{c_{out}}\right\}$, and σ_w defined as above, we have*

$$\text{Var}\left(\frac{w_{ij}}{\sigma_w}\right) \leq \frac{2}{c_{in} k_w k_h + c_{out} k_w k_h}.$$

Furthermore, if $c_{in}, c_{out} \geq 2$ and $c_{in} k_w k_h, c_{out} k_w k_h \geq 3$, and w_{ij} are from a zero-mean Gaussian distribution, there exists a constant L that does not depend on $c_{in}, c_{out}, k_w, k_h$ such that

$$\frac{L}{c_{in} k_w k_h \log(c_{out}) + c_{out} k_w k_h \log(c_{in})} \leq \text{Var}\left(\frac{w_{ij}}{\sigma_w}\right) \leq \frac{2}{c_{in} k_w k_h + c_{out} k_w k_h}.$$

(Proof in App. G). Note that in convolution layers, $n_i = c_{in} k_w k_h$ and $m_i = c_{out} k_w k_h$. Therefore, BSN sets the variance of parameters to scale as $\frac{2}{n_i+m_i}$, as dictated by Xavier initialization. Moreover, BSN naturally inherits the benefits of SN discussed in § 4 (e.g. insensitive to initialization parameters, controlling variance throughout the training).

5.1 Results

Since SN is widely regarded as one of the most successful normalization techniques for GANs [10, 39, 5] and our proposed BSN is meant to improve SN, we compare the performance of SN and BSN. In addition, we compare against two variants of SN proposed in the appendix of [25], which we denote “same γ ” and “diff. γ ” (details in App. M). The standard SN from [25] is denoted by “no γ ”. We run experiments on CIFAR10, STL10, CelebA, and ImageNet, with two widely-used metrics for sample quality: inception score [34] and Frechet Inception Distance (FID) [15] (details in App. H). The code for reproducing all experiments can be found in <https://github.com/fjxmlzn/BSN>.

CIFAR10, STL10, and CelebA. We use the network architecture from SN [25]. We controlled five hyperparameters (Table 7, App. N): α_g and α_d , the generator/discriminator learning rates, β_1, β_2 , Adam momentum parameters [18], and n_{dis} , the number of discriminator updates per generator update. Three hyperparameter settings are from [25], with equal discriminator and generator learning rates; the final two test *unequal* learning rates. More details are in Apps. N and O.

As in [25], we report the metrics from the best hyperparameter for each algorithm in Table 1. *BSN outperforms the standard SN in all sample quality metrics except FID score on STL10, where their metrics are within standard error of each other.* Regarding the SN variants, in CIFAR10 and STL10, they have worse performance than SN and BSN, same as reported in [25]. In CelebA, the SN variants have better performance for the best hyperparameter setting. But in general, these SN variants are very sensitive to hyperparameters (Apps. N to P), therefore they are not adopted in practice [25].

More importantly, the superiority of BSN is stable across hyperparameters. Figs. 8 and 9 show the inception scores of all the hyperparameters we tested on CIFAR10 and STL10. BSN has the best or

	CIFAR10		STL10		CelebA
	Inception score	FID	Inception score	FID	FID
Real data	11.26	9.70	26.70	10.17	4.44
SN (no γ , [25])	7.22 ± 0.09	31.43 ± 0.90	9.16 ± 0.03	42.89 ± 0.54	9.09 ± 0.32
SN (same γ)	6.46 ± 0.06	42.35 ± 0.74	8.86 ± 0.03	54.61 ± 0.51	7.74 ± 0.11
SN (diff. γ)	6.53 ± 0.01	41.88 ± 0.50	8.79 ± 0.03	56.76 ± 0.44	7.54 ± 0.08
BSN (ours)	7.58 ± 0.04	26.62 ± 0.21	9.25 ± 0.01	42.98 ± 0.54	8.54 ± 0.20

Table 1: Inception scores and FIDs on CIFAR10, STL10, and CelebA. Each experiment is conducted with 5 random seeds, with mean and standard error reported. We follow the common practice of excluding Inception Score in CelebA as the inception network is pretrained on ImageNet, which is very different from CelebA. “no γ ” denotes the standard spectral normalization used in practice, whereas “same γ ” and “diff. γ ” are variants proposed in the appendix of [25].

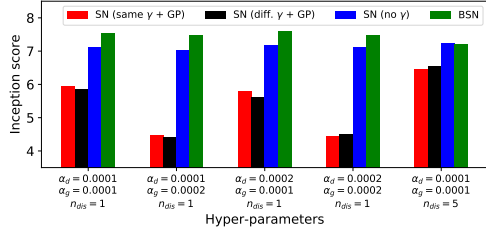


Figure 8: Inception score in CIFAR10. The results are averaged over 5 random seeds.

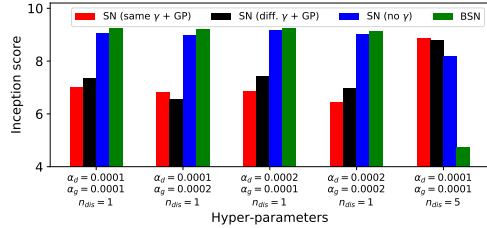


Figure 9: Inception score in STL10. The results are averaged over 5 random seeds.

competitive performance in most of the settings. The only exception is $n_{dis} = 5$ setting in STL10, where we observe that the performance from both SN and BSN have larger variance across different random seeds, and the SN variants with γ perform better. On CelebA, BSN also outperforms SN in FID across all hyperparameters (App. P), and it outperforms all SN variants in every hyperparameter setting except one (Fig. 52).

Moreover, we see that as training proceeds, the sample quality of SN often drops, whereas the sample quality of BSN appears to monotonically increase (Fig. 7, more in Apps.). In most cases, BSN not only outperforms SN in final sample quality (after training), but also in *peak* sample quality. This means that BSN makes the training process more stable, which is the purpose of SN (and BSN). More results (generated images, training curves, FID plots) are in Apps. N to P.

ImageNet. To further test if BSN scales to large-scale dataset and larger network, we compare SN and BSN in ILSVRC2012 dataset. We take the same ResNet-based architectures [14] and hyperparameter settings as in [25], which we reproduced in App. Q.

We found that BSN without any tuning has the same gradient vanishing problem we observe for SN_{Conv} [8] in § 4. We hypothesize that this is because of the distinction between ResNet and our analysis in § 4 and 5, which does not account for shortcut connections. The optimal variance and scaling for BSN (and for SN) in ResNet-based architectures might be different from our results in § 4 and 5. We defer theoretical analysis of ResNets to future work.

To verify that the gradient vanishing is caused by the wrong scaling, we apply the scaling techniques introduced in § 4 for BSN, and find that this successfully solves the gradient vanishing problem. Table 2 shows the results of SN and BSN with different scale parameters. We see that the sample quality of scaled BSN outperforms the SN without scaling by a large margin. To verify that this benefit is from the formulation of BSN instead of the scaling, we also apply scaling over SN. From the table we see that for all the scales that are larger than 1 we try, BSN always outperforms SN. The best BSN (with scale=1.4) outperforms the best SN (with scale=1.0/1.4) by a large margin. In fact, applying scaling on SN does not make noticeable improvement on the sample quality, and could even

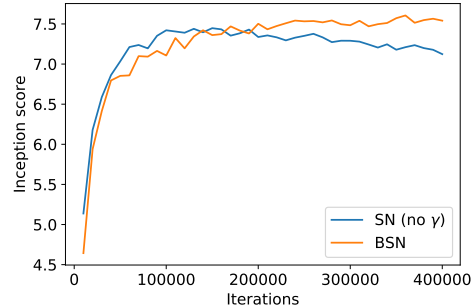


Figure 7: Inception score in CIFAR10. The results are averaged over 5 random seeds, with $\alpha_g = 0.0001$, $\alpha_d = 0.0001$, $n_{dis} = 1$.

make it worse (e.g. when scale=1.6). This accords with the phenomenon we observed in § 4. More results (e.g. samples, training curves) are in App. Q.

6 Discussion and Related Work

Our results suggest that SN stabilizes GANs by controlling exploding and vanishing gradients in the discriminator. However, our analysis applies to the training of any fully-connected, feed-forward neural network. This connection partially explains why SN helps train generators as well as discriminators [44, 5], and why SN is more generally useful in training neural networks [8, 12, 42]. Formally extending this analysis to understand the effects of adversarial training is an interesting direction for future work. The other future direction is to propose an even better regularization technique where the variance is exactly $\frac{2}{n_i+m_i}$, as our approach only gives a range for the variance.

A related result to our upper bound was shown in [36], which shows that batch normalization (BN) makes the scaling of the Hessian along the direction of the gradient smaller, thereby making gradients more predictive. Given Prop. 1, we can apply the reasoning from [36] to explain why spectrally-normalized GANs are robust to different learning rates as shown in [25]. However, our insights regarding the gradient vanishing problem are the more surprising result; this notion is not discussed in [36]. An interesting question for future work is whether BN similarly controls vanishing gradients.

References

- [1] Martin Arjovsky and Léon Bottou. Towards principled methods for training generative adversarial networks, 2017.
- [2] Martin Arjovsky, Soumith Chintala, and Léon Bottou. Wasserstein gan. *arXiv preprint arXiv:1701.07875*, 2017.
- [3] Peter L Bartlett, Dylan J Foster, and Matus J Telgarsky. Spectrally-normalized margin bounds for neural networks. In *Advances in Neural Information Processing Systems*, pages 6240–6249, 2017.
- [4] Yoshua Bengio, Patrice Simard, and Paolo Frasconi. Learning long-term dependencies with gradient descent is difficult. *IEEE transactions on neural networks*, 5(2):157–166, 1994.
- [5] Andrew Brock, Jeff Donahue, and Karen Simonyan. Large scale gan training for high fidelity natural image synthesis. *arXiv preprint arXiv:1809.11096*, 2018.
- [6] Andrew Brock, Theodore Lim, James M Ritchie, and Nick Weston. Neural photo editing with introspective adversarial networks. *arXiv preprint arXiv:1609.07093*, 2016.
- [7] Adam Coates, Andrew Ng, and Honglak Lee. An analysis of single-layer networks in unsupervised feature learning. In *Proceedings of the fourteenth international conference on artificial intelligence and statistics*, pages 215–223, 2011.
- [8] Farzan Farnia, Jesse M Zhang, and David Tse. Generalizable adversarial training via spectral normalization. *arXiv preprint arXiv:1811.07457*, 2018.
- [9] Xavier Glorot and Yoshua Bengio. Understanding the difficulty of training deep feedforward neural networks. In *Proceedings of the thirteenth international conference on artificial intelligence and statistics*, pages 249–256, 2010.

Scale	Approach	Inception score	FID
1.0	SN	12.84 ± 0.33	75.06 ± 2.38
	BSN (ours)	1.77 ± 0.13	265.20 ± 19.01
1.2	SN	12.73 ± 0.13	74.10 ± 1.41
	BSN (ours)	13.23 ± 0.19	71.53 ± 1.92
1.4	SN	12.76 ± 0.17	73.21 ± 1.92
	BSN (ours)	13.23 ± 0.16	69.04 ± 1.46
1.6	SN	11.53 ± 0.49	81.33 ± 5.51
	BSN (ours)	13.01 ± 0.12	71.56 ± 1.18

Table 2: Inception scores and FIDs on ILSVRC2012. SN with scale=1.0 is conducted with 5 random seeds, and all others are conducted with 3 random seeds, with mean and standard error reported. The bold font marks the best numbers between SN and BSN using a specific scale. The red color marks the best numbers among all runs.

- [10] Xinyu Gong, Shiyu Chang, Yifan Jiang, and Zhangyang Wang. Autogan: Neural architecture search for generative adversarial networks. In *Proceedings of the IEEE International Conference on Computer Vision*, pages 3224–3234, 2019.
- [11] Ian Goodfellow, Jean Pouget-Abadie, Mehdi Mirza, Bing Xu, David Warde-Farley, Sherjil Ozair, Aaron Courville, and Yoshua Bengio. Generative adversarial nets. In *Advances in neural information processing systems*, pages 2672–2680, 2014.
- [12] Henry Gouk, Eibe Frank, Bernhard Pfahringer, and Michael Cree. Regularisation of neural networks by enforcing lipschitz continuity. *arXiv preprint arXiv:1804.04368*, 2018.
- [13] Ishaan Gulrajani, Faruk Ahmed, Martin Arjovsky, Vincent Dumoulin, and Aaron C Courville. Improved training of wasserstein gans. In *Advances in neural information processing systems*, pages 5767–5777, 2017.
- [14] Kaiming He, Xiangyu Zhang, Shaoqing Ren, and Jian Sun. Deep residual learning for image recognition. In *Proceedings of the IEEE conference on computer vision and pattern recognition*, pages 770–778, 2016.
- [15] Martin Heusel, Hubert Ramsauer, Thomas Unterthiner, Bernhard Nessler, and Sepp Hochreiter. Gans trained by a two time-scale update rule converge to a local nash equilibrium. In *Advances in neural information processing systems*, pages 6626–6637, 2017.
- [16] Alexia Jolicoeur-Martineau. The relativistic discriminator: a key element missing from standard gan. *arXiv preprint arXiv:1807.00734*, 2018.
- [17] Tero Karras, Timo Aila, Samuli Laine, and Jaakko Lehtinen. Progressive growing of gans for improved quality, stability, and variation. *arXiv preprint arXiv:1710.10196*, 2017.
- [18] Diederik P Kingma and Jimmy Ba. Adam: A method for stochastic optimization. *arXiv preprint arXiv:1412.6980*, 2014.
- [19] Alex Krizhevsky, Geoffrey Hinton, et al. Learning multiple layers of features from tiny images. 2009.
- [20] Yann LeCun, Leon Bottou, Genevieve B. Orr, and Klaus Robert Müller. *Efficient BackProp*, pages 9–50. Springer Berlin Heidelberg, Berlin, Heidelberg, 1998.
- [21] Yann LeCun and Corinna Cortes. MNIST handwritten digit database. 2010.
- [22] Alex X Lee, Richard Zhang, Frederik Ebert, Pieter Abbeel, Chelsea Finn, and Sergey Levine. Stochastic adversarial video prediction. *arXiv preprint arXiv:1804.01523*, 2018.
- [23] Zinan Lin, Kiran Koshy Thekumparampil, Giulia Fanti, and Sewoong Oh. Infogan-cr: Disentangling generative adversarial networks with contrastive regularizers. *arXiv preprint arXiv:1906.06034*, 2019.
- [24] Ziwei Liu, Ping Luo, Xiaogang Wang, and Xiaoou Tang. Deep learning face attributes in the wild. In *Proceedings of International Conference on Computer Vision (ICCV)*, December 2015.
- [25] Takeru Miyato, Toshiki Kataoka, Masanori Koyama, and Yuichi Yoshida. Spectral normalization for generative adversarial networks. *arXiv preprint arXiv:1802.05957*, 2018.
- [26] Takeru Miyato and Masanori Koyama. cgans with projection discriminator. *arXiv preprint arXiv:1802.05637*, 2018.
- [27] Behnam Neyshabur, Srinadh Bhojanapalli, and Nathan Srebro. A pac-bayesian approach to spectrally-normalized margin bounds for neural networks. *arXiv preprint arXiv:1707.09564*, 2017.
- [28] Augustus Odena, Jacob Buckman, Catherine Olsson, Tom Brown, Christopher Olah, Colin Raffel, and Ian Goodfellow. Is generator conditioning causally related to gan performance? In *International Conference on Machine Learning*, pages 3849–3858, 2018.
- [29] Razvan Pascanu, Tomas Mikolov, and Yoshua Bengio. Understanding the exploding gradient problem. *CoRR, abs/1211.5063*, 2:417, 2012.
- [30] Razvan Pascanu, Tomas Mikolov, and Yoshua Bengio. On the difficulty of training recurrent neural networks. In *International conference on machine learning*, pages 1310–1318, 2013.
- [31] Jeffrey Pennington, Samuel Schoenholz, and Surya Ganguli. Resurrecting the sigmoid in deep learning through dynamical isometry: theory and practice. In *Advances in neural information processing systems*, pages 4785–4795, 2017.

- [32] Alec Radford, Luke Metz, and Soumith Chintala. Unsupervised representation learning with deep convolutional generative adversarial networks. *arXiv preprint arXiv:1511.06434*, 2015.
- [33] Olga Russakovsky, Jia Deng, Hao Su, Jonathan Krause, Sanjeev Satheesh, Sean Ma, Zhiheng Huang, Andrej Karpathy, Aditya Khosla, Michael Bernstein, Alexander C. Berg, and Li Fei-Fei. ImageNet Large Scale Visual Recognition Challenge. *International Journal of Computer Vision (IJCV)*, 115(3):211–252, 2015.
- [34] Tim Salimans, Ian Goodfellow, Wojciech Zaremba, Vicki Cheung, Alec Radford, and Xi Chen. Improved techniques for training gans. In *Advances in neural information processing systems*, pages 2234–2242, 2016.
- [35] Tim Salimans and Durk P Kingma. Weight normalization: A simple reparameterization to accelerate training of deep neural networks. In *Advances in neural information processing systems*, pages 901–909, 2016.
- [36] Shibani Santurkar, Dimitris Tsipras, Andrew Ilyas, and Aleksander Madry. How does batch normalization help optimization? In *Advances in Neural Information Processing Systems*, pages 2483–2493, 2018.
- [37] Yoav Seginer. The expected norm of random matrices. *Combinatorics, Probability and Computing*, 9(2):149–166, 2000.
- [38] Yusuke Tsuzuku, Issei Sato, and Masashi Sugiyama. Lipschitz-margin training: Scalable certification of perturbation invariance for deep neural networks. In *Advances in Neural Information Processing Systems*, pages 6541–6550, 2018.
- [39] Wei Wang, Yuan Sun, and Saman Halgamuge. Improving mmd-gan training with repulsive loss function. *arXiv preprint arXiv:1812.09916*, 2018.
- [40] David Warde-Farley and Yoshua Bengio. Improving generative adversarial networks with denoising feature matching. 2016.
- [41] Xiang Wei, Boqing Gong, Zixia Liu, Wei Lu, and Liqiang Wang. Improving the improved training of wasserstein gans: A consistency term and its dual effect. *arXiv preprint arXiv:1803.01541*, 2018.
- [42] Yuichi Yoshida and Takeru Miyato. Spectral norm regularization for improving the generalizability of deep learning. *arXiv preprint arXiv:1705.10941*, 2017.
- [43] Jiahui Yu, Zhe Lin, Jimei Yang, Xiaohui Shen, Xin Lu, and Thomas S Huang. Free-form image inpainting with gated convolution. In *Proceedings of the IEEE International Conference on Computer Vision*, pages 4471–4480, 2019.
- [44] Han Zhang, Ian Goodfellow, Dimitris Metaxas, and Augustus Odena. Self-attention generative adversarial networks. *arXiv preprint arXiv:1805.08318*, 2018.

Appendix

A Proof of Prop. 1

The proposition makes use of the following observation: For the discriminator defined in (1), the norm of gradient for w_t is upper bounded by

$$\|\nabla_{w_t} D_\theta(x)\|_F \leq \|x\| \cdot \prod_{i=1}^L \|a_i\|_{\text{Lip}} \cdot \prod_{i=1}^L \|w_i\|_{\text{sp}} / \|w_t\|_{\text{sp}} \quad \text{for } \forall t \in [1, L] \quad (6)$$

To prove this, for simplicity of notation, let $o_a^i = a_i \circ l_{w_i} \circ \dots \circ a_1 \circ l_{w_1}$, and $o_l^i = l_{w_i} \circ a_{i-1} \circ \dots \circ a_1 \circ l_{w_1}$.

It is straightforward to show that the norm of each internal output of discriminator is bounded by

$$\|o_a^t(x)\| \leq \|x\| \cdot \prod_{i=1}^t \|a_i\|_{\text{Lip}} \cdot \prod_{i=1}^t \|w_i\|_{\text{sp}} \quad (7)$$

and

$$\|o_l^t(x)\| \leq \|x\| \cdot \prod_{i=1}^{t-1} \|a_i\|_{\text{Lip}} \cdot \prod_{i=1}^t \|w_i\|_{\text{sp}}. \quad (8)$$

This holds because

$$\|o_a^t(x)\| = \|a_i(o_l^t(x))\| \leq \|a_i\|_{\text{Lip}} \cdot \|o_l^t(x)\|$$

and

$$\|o_l^t(x)\| = \|l_{w_i}(o_a^{t-1}(x))\| \leq \|w_t\|_{\text{sp}} \cdot \|o_a^{t-1}(x)\|,$$

from which we can show the desired inequalities by induction.

Next, we observe that the norm of each internal gradient is bounded by

$$\|\nabla_{o_a^t(x)} D_\theta(x)\| \leq \prod_{i=t+1}^L \|a_i\|_{\text{Lip}} \cdot \prod_{i=t+1}^L \|w_i\|_{\text{sp}} \quad (9)$$

and

$$\|\nabla_{o_l^t(x)} D_\theta(x)\| \leq \prod_{i=t}^L \|a_i\|_{\text{Lip}} \cdot \prod_{i=t+1}^L \|w_i\|_{\text{sp}}. \quad (10)$$

This holds because

$$\|\nabla_{o_a^t(x)} D_\theta(x)\| = \|w_{t+1}^T \nabla_{o_l^{t+1}(x)} D_\theta(x)\| \leq \|w_{t+1}\|_{\text{sp}} \|\nabla_{o_l^{t+1}(x)} D_\theta(x)\|$$

and

$$\|\nabla_{o_l^t(x)} D_\theta(x)\| = \left\| \langle \nabla_{o_a^t(x)} D_\theta(x), [a_t'(x)|_{x=o_l^t(x)}] \rangle \right\| \leq \|a_t\|_{\text{Lip}} \|\nabla_{o_a^t(x)} D_\theta(x)\|,$$

from which we can show inequalities Eqs. (9) and (10) by induction.

Now we have that

$$\begin{aligned} \|\nabla_{w_t} D_\theta(x)\|_F &= \left\| \nabla_{o_l^t(x)} D_\theta(x) \cdot (o_a^{t-1}(x))^T \right\|_F \\ &= \left\| \nabla_{o_l^t(x)} D_\theta(x) \right\| \cdot \|o_a^{t-1}(x)\| \\ &\leq \prod_{i=t}^L \|a_i\|_{\text{Lip}} \cdot \prod_{i=t+1}^L \|w_i\|_{\text{sp}} \cdot \|x\| \cdot \prod_{i=1}^{t-1} \|a_i\|_{\text{Lip}} \cdot \prod_{i=1}^{t-1} \|w_i\|_{\text{sp}} \\ &= \|x\| \cdot \prod_{i=1}^L \|a_i\|_{\text{Lip}} \cdot \prod_{i=1}^L \|w_i\|_{\text{sp}} / \|w_t\|_{\text{sp}} \end{aligned}$$

where we use Eqs. (7) to (10) at the inequality. The upper bound of gradient's Frobenius norm for spectrally-normalized discriminators follows directly.

B Proof of Prop. 2

Proof. As $l_w(x)$ is a linear transformation, we have $l_{cw}(x) = c \cdot l_w(x)$, and $l_w(cx) = c \cdot l_w(x)$. Moreover, since ReLU and leaky ReLU is linear in \mathbb{R}^+ and \mathbb{R}^- region, we have $a_i(cx) = c \cdot a_i(x)$. Therefore, we have

$$\begin{aligned} D'_\theta(x) &= (a_L \circ l_{c_L \cdot w_L} \circ a_{L-1} \circ l_{c_{L-1} \cdot w_{L-1}} \circ \dots \circ a_1 \circ l_{c_1 \cdot w_1})(x) \\ &= \prod_{i=1}^L c_i \cdot (a_L \circ l_{w_L} \circ a_{L-1} \circ l_{w_{L-1}} \circ \dots \circ a_1 \circ l_{w_1})(x) \\ &= D_\theta(x) \end{aligned}$$

□

C Additional Analysis of Gradient

In § 3, we discuss the gradients with respect to $w'_i = \frac{w_i}{u_i^T w_i v_i}$, where u_i, v_i are the singular vectors corresponding to the largest singular values. In this section we discuss the gradients with respect to the actual parameter w_i . From Eq. (12) in [25] we know

$$\nabla_{w_t} D_\theta(x) = \frac{1}{\|w_t\|_{\text{sp}}} \left(\nabla_{w'_t} D_\theta(x) - \left(\left(\nabla_{o_t^t(x)} D_\theta(x) \right)^T o_t^t(x) \right) \cdot u_t v_t^T \right)$$

From App. A, we know that $\|\nabla_{w'_t} D_\theta(x)\|_{\text{F}}$, $\|\nabla_{o_t^t(x)} D_\theta(x)\|$, and $\|o_t^t(x)\|$ have upper bounds. Furthermore, $\|u_t v_t^T\|_{\text{F}} = 1$. Therefore, $\left\| \nabla_{w'_t} D_\theta(x) - \left(\left(\nabla_{o_t^t(x)} D_\theta(x) \right)^T o_t^t(x) \right) \cdot u_t v_t^T \right\|_{\text{F}}$ has an upper bound. From Theorem 1.1 in [37] we know that if w_t is initialized with i.i.d random variables from uniform or Gaussian distribution, $\mathbb{E}(\|w_t\|_{\text{sp}})$ is lower bounded away from zero at initialization. So $\|\nabla_{w_t} D_\theta(x)\|_{\text{F}}$ is upper bounded at initialization. Moreover, we observe empirically that $\|w_t\|_{\text{sp}}$ is usually increasing during training. Therefore, $\|\nabla_{w_t} D_\theta(x)\|_{\text{F}}$ is typically upper bounded during training as well.

D Analysis of Hessian

The following proposition states that spectral normalization also gives an upper bound on $\|H_{w_i}(D_\theta)(x)\|_{\text{sp}}$ for networks with ReLU or leaky ReLU internal activations.

Proposition 3 (Upper bound of Hessian's spectral norm). *Consider the discriminator defined in Eq. (1). Let $H_{w_i}(D_\theta)(x)$ denote the Hessian of D_θ at x with respect with the vector form of w_i . If the internal activations are ReLU or leaky ReLU, the spectral norm of $H_{w_i}(D_\theta)(x)$ is upper bounded by*

$$\|H_{w_i}(D_\theta)(x)\|_{\text{sp}} \leq \left\| H_{o_i^t(x)} D_\theta(x) \right\|_{\text{sp}} \cdot \|x\|^2 \cdot \prod_{i=1}^L \|w_i\|_{\text{sp}}^2 / \|w_t\|_{\text{sp}}^2$$

The proof is in App. D.1. Following Prop. 3, we can easily show the upper bound of Hessian's spectral norm for spectral normalized discriminators.

Corollary 1 (Upper bound of Hessian's spectral norm for spectral normalization). *If the internal activations are ReLU or leaky ReLU, and $\|w_i\|_{\text{sp}} \leq 1$ for all $i \in [1, L]$, then*

$$\|H_{w_i}(D_\theta)(x)\|_{\text{sp}} \leq \left\| H_{o_i^t(x)} D_\theta(x) \right\|_{\text{sp}} \cdot \|x\|^2 .$$

Moreover, if the activation for the last layer is sigmoid (e.g., for vanilla GAN [11]), we have

$$\|H_{w_i}(D_\theta)(x)\|_{\text{sp}} \leq 0.1 \|x\|^2 ;$$

if the activation function for the last layer is identity (e.g., for WGAN-GP [13]), we have

$$\|H_\theta(D_\theta)(x)\|_{\text{sp}} = 0 .$$

D.1 Proof of Prop. 3

Lemma 1. *The spectral norm of each internal Hessian is bounded by*

$$\|H_{o_a^t(x)} D_\theta(x)\|_{\text{sp}} \leq \|H_{o_l^L(x)} D_\theta(x)\|_{\text{sp}} \cdot \prod_{i=t+1}^L \|w_i\|_{\text{sp}}^2$$

and

$$\|H_{o_l^t(x)} D_\theta(x)\|_{\text{sp}} \leq \|H_{o_l^L(x)} D_\theta(x)\|_{\text{sp}} \cdot \prod_{i=t+1}^L \|w_i\|_{\text{sp}}^2$$

Proof. We have

$$\begin{aligned} \|H_{o_a^t(x)} D_\theta(x)\|_{\text{sp}} &= \left\| w_{t+1}^T \cdot \nabla_{o_l^{t+1}(x)} D_\theta(x) \cdot w_{t+1} \right\|_{\text{sp}} \\ &\leq \left\| \nabla_{o_l^{t+1}(x)} D_\theta(x) \right\|_{\text{sp}} \|w_{t+1}\|_{\text{sp}}^2. \end{aligned}$$

We also have

$$\begin{aligned} \left\| H_{o_l^t(x)} D_\theta(x) \right\|_{\text{sp}} &= \left\| \text{diag}([a'_t(x)]_{x=o_a^t(x)}) \cdot H_{o_a^{t+1}(x)} D_\theta(x) \cdot \text{diag}([a'_t(x)]_{x=o_a^t(x)}) \right\|_{\text{sp}} \\ &\leq \left\| H_{o_a^{t+1}(x)} D_\theta(x) \right\|_{\text{sp}} \end{aligned}$$

where we use the property that ReLU or leaky ReLU is piece-wise linear. The desired inequalities then follow by induction. \square

Now let's come back to the proof for Prop. 3.

Proof. We have

$$\frac{\partial D_\theta}{\partial (w_t)_{ij} \partial (w_t)_{kl}} = \left(H_{o_l^t}(D_\theta)(x) \right)_{ik} \cdot (o_a^{t-1}(x))_j \cdot (o_a^{t-1}(x))_l.$$

Therefore,

$$\|H_{w_i}(D_\theta)(x)\|_{\text{sp}} \leq \|H_{o_l^t}(D_\theta)(x)\|_{\text{sp}} \|o_a^{t-1}(x)\|_\infty^2 \leq \|H_{o_l^t}(D_\theta)(x)\|_{\text{sp}} \|o_a^{t-1}(x)\|^2$$

Applying Eq. (7) and Lemma 1 we get

$$\begin{aligned} \|H_{w_i}(D_\theta)(x)\|_{\text{sp}} &\leq \|H_{o_l^t(x)} D_\theta(x)\|_{\text{sp}} \cdot \prod_{i=t+1}^L \|w_i\|_{\text{sp}}^2 \cdot \|x\|^2 \cdot \prod_{i=1}^{t-1} \|w_i\|_{\text{sp}}^2 \\ &= \|H_{o_l^t(x)} D_\theta(x)\|_{\text{sp}} \cdot \|x\|^2 \cdot \prod_{i=1}^L \|w_i\|_{\text{sp}}^2 / \|w_t\|_{\text{sp}}^2 \end{aligned}$$

\square

E Proof of Thm. 1

Proof. For any discriminator $D_\theta = a_L \circ l_{w_L} \circ a_{L-1} \circ l_{w_{L-1}} \circ \dots \circ a_1 \circ l_{w_1}$, consider $\theta' = \left\{ w'_t \triangleq c_t w_t \right\}_{t=1}^L$ with the constraint $\prod_{i=1}^L c_i = 1$ and $c_i \in \mathbb{R}^+$. Let $Q = \left\| \nabla_{w'_i} D_{\theta'}(x) \right\|_{\text{F}} \|w'_i\|_{\text{sp}}$.

We have

$$\begin{aligned}
\|\nabla_{\theta'} D_{\theta'}(x)\|_{\text{F}} &= \sqrt{\sum_{i=1}^L \|\nabla_{w_i'} D_{\theta'}(x)\|_{\text{F}}^2} \\
&= \sqrt{\sum_{i=1}^L \frac{Q^2}{c_i^2 \|w_i\|_{\text{sp}}^2}} \\
&\geq \sqrt{L \left(\prod_{i=1}^L \frac{Q^2}{c_i^2 \|w_i\|_{\text{sp}}^2} \right)^{1/L}} \\
&= \sqrt{L} \cdot Q^{1/L} \cdot \left(\prod_{i=1}^L \|w_i\|_{\text{sp}} \right)^{-1/L}
\end{aligned}$$

and the equality is achieved iff $c_i^2 \|w_i\|_{\text{sp}}^2 = c_j^2 \|w_j\|_{\text{sp}}^2$, $\forall i, j \in [1, L]$ according to AM-GM inequality. When $c_i^2 \|w_i\|_{\text{sp}}^2 = c_j^2 \|w_j\|_{\text{sp}}^2$, $\forall i, j \in [1, L]$, we have $c_t = \prod_{i=1}^L \|w_i\|_{\text{sp}}^{1/L} / \|w_t\|_{\text{sp}}$. \square

F Proof of Thm. 2

Proof. Since a_{ij} are symmetric random variables, we know $\mathbb{E} \left(\frac{a_{ij}}{\|A\|_{\text{sp}}} \right) = 0$. Further, by symmetry, we have that for any $(i, j) \neq (h, \ell)$, $\mathbb{E} \left(\frac{a_{ij}^2}{\|A\|_{\text{sp}}^2} \right) = \mathbb{E} \left(\frac{a_{h\ell}^2}{\|A\|_{\text{sp}}^2} \right)$. Therefore, we have

$$\text{Var} \left(\frac{a_{ij}}{\|A\|_{\text{sp}}} \right) = \mathbb{E} \left(\frac{a_{ij}^2}{\|A\|_{\text{sp}}^2} \right) = \frac{1}{mn} \cdot \mathbb{E} \left(\frac{\sum_{i=1}^m \sum_{j=1}^n a_{ij}^2}{\|A\|_{\text{sp}}^2} \right) = \frac{1}{mn} \cdot \mathbb{E} \left(\frac{\|A\|_{\text{F}}^2}{\|A\|_{\text{sp}}^2} \right)$$

Our approach will be to upper and lower bound the quantity $\frac{1}{mn} \cdot \mathbb{E} \left(\frac{\|A\|_{\text{F}}^2}{\|A\|_{\text{sp}}^2} \right)$.

Upper bound Assume the singular values of A are $\sigma_1 \geq \sigma_2 \geq \dots \geq \sigma_{\min\{m,n\}}$. We have

$$\frac{1}{mn} \cdot \mathbb{E} \left(\frac{\|A\|_{\text{F}}^2}{\|A\|_{\text{sp}}^2} \right) = \frac{1}{mn} \cdot \mathbb{E} \left(\frac{\sum_{i=1}^{\min\{m,n\}} \sigma_i^2}{\sigma_1^2} \right) \leq \frac{\min\{m, n\}}{mn} = \frac{1}{\max\{m, n\}},$$

which gives the desired upper bound.

Lower bound Now for the lower bound, if a_{ij} are drawn from zero-mean Gaussian distribution and $\max\{m, n\} \geq 3$, we have

$$\frac{1}{mn} \cdot \mathbb{E} \left(\frac{\|A\|_{\text{F}}^2}{\|A\|_{\text{sp}}^2} \right) \tag{11}$$

$$\begin{aligned}
&= \frac{1}{mn} \cdot \mathbb{E} \left(\frac{1}{\|A\|_{\text{sp}}^2 / \|A\|_{\text{F}}^2} \right) \\
&\geq \frac{1}{mn} \cdot \frac{1}{\mathbb{E} \left(\left\| \frac{A}{\|A\|_{\text{F}}} \right\|_{\text{sp}}^2 \right)} \\
&= \frac{1}{mn} \cdot \frac{1}{\mathbb{E} \left(\|B\|_{\text{sp}}^2 \right)} \tag{12}
\end{aligned}$$

where $B \in R^{m \times n}$ is uniformly sampled from the sphere of $m \times n$ -dimension unit ball. We use the following lemma to lower bound (12).

Lemma 2 (Theorem 1.1 in [37]). Assume $A \in \mathbb{R}^{m \times n}$ is uniformly sampled from the sphere of $m \times n$ -dimension unit ball. When $\max\{m, n\} \geq 3$, we have

$$\mathbb{E} \left(\|A\|_{sp}^2 \right) \leq K^2 \left(\mathbb{E} \left(\max_{1 \leq i \leq m} \|a_{i\bullet}\|^2 \right) + \mathbb{E} \left(\max_{1 \leq j \leq n} \|a_{\bullet j}\|^2 \right) \right),$$

where K is a constant which does not depend on m, n . Here $a_{i\bullet}$ denotes the i -th row of A , and $a_{\bullet j}$ denotes the j -th column of A .¹

We thus have that

$$\frac{1}{mn} \cdot \frac{1}{\mathbb{E} \left(\|B\|_{sp}^2 \right)} \geq \frac{1}{mn} \cdot \frac{1}{K^2 \left(\mathbb{E} \left(\max_{1 \leq i \leq m} \|b_{i\bullet}\|^2 \right) + \mathbb{E} \left(\max_{1 \leq j \leq n} \|b_{\bullet j}\|^2 \right) \right)}.$$

Hence, we need to upper bound $\mathbb{E} \left(\max_{1 \leq i \leq m} \|b_{i\bullet}\|^2 \right)$ and $\mathbb{E} \left(\max_{1 \leq j \leq n} \|b_{\bullet j}\|^2 \right)$. Let $z \in \mathbb{R}^m$ be a vector uniformly sampled from the sphere of m -dimension unit ball. Observe that $z \stackrel{d}{=} [\|b_{1\bullet}\|, \dots, \|b_{m\bullet}\|]$. The following lemma upper bounds the square of the infinity norm of this vector.

Lemma 3. Assume $z = [z_1, z_2, \dots, z_n]$ is uniformly sampled from the sphere of n -dimension unit ball, where $n \geq 2$. Then we have

$$\mathbb{E} \left(\max_{1 \leq i \leq n} z_i^2 \right) \leq \frac{4 \log(n)}{n-1}.$$

(Proof in App. F.1)

Hence, when $m, n \geq 2$, we have

$$\mathbb{E} \left(\max_{1 \leq i \leq m} \|b_{i\bullet}\|^2 \right) \leq \frac{4 \log(m)}{m-1}$$

Similarly, we have

$$\mathbb{E} \left(\max_{1 \leq j \leq n} \|b_{\bullet j}\|^2 \right) \leq \frac{4 \log(n)}{n-1}$$

Therefore,

$$\begin{aligned} & \text{Var} \left(\frac{a_{ij}}{\|A\|_{sp}} \right) \\ & \geq \frac{1}{mn} \cdot \frac{1}{K^2 \left(\frac{4 \log(m)}{m-1} + \frac{4 \log(n)}{n-1} \right)} \\ & \geq \frac{1}{8K^2} \cdot \frac{1}{n \log(m) + m \log(n)} \\ & \geq \frac{1}{16K^2} \cdot \frac{1}{\max\{m, n\} \log(\min\{m, n\})} \end{aligned}$$

which gives the result. □

¹Note that the original theorem in [37] requires that the entries of A be i.i.d. symmetric random variables, whereas in our case the entries are not i.i.d., as we require $\|A\|_F = 1$. However, the i.i.d. assumption in their proof is only used to ensure that A , $S_{\sigma^{(1)}, \epsilon^{(1)}}(A)$, and $S_{\sigma^{(2)}, \epsilon^{(2)}}(A)$ have the same distribution, where $\sigma^{(t)}$ for $t = 0, 1$ are vectors of independent random permutations; $\epsilon^{(t)}$ for $t = 0, 1$ are matrices of i.i.d. random variables with equal probability of being ± 1 ; and $S_{\sigma^{(1)}, \epsilon^{(1)}}(A) = \left(\epsilon_{ij}^{(1)} \cdot a_{i, \sigma_i^{(1)}(j)} \right)_{i,j}$ and $S_{\sigma^{(2)}, \epsilon^{(2)}}(A) = \left(\epsilon_{ij}^{(2)} \cdot a_{\sigma_j^{(2)}(i), j} \right)_{i,j}$. Our matrix A satisfies this requirement, and therefore the same theorem holds.

F.1 Proof of Lemma 3

Proof.

$$\begin{aligned}
& \mathbb{E} \left(\max_{1 \leq i \leq n} z_i^2 \right) \\
&= \int_0^1 \mathbb{P} \left(\max_{1 \leq i \leq n} z_i^2 \geq \delta \right) d\delta \\
&\leq \int_0^1 \min \{1, n \cdot \mathbb{P}(z_1^2 \geq \delta)\} d\delta
\end{aligned} \tag{13}$$

where (13) follows from the union bound. Next, we use the following lemma to upper bound $\mathbb{P}(z_1^2 \geq \delta)$.

Lemma 4. *Assume $z = [z_1, z_2, \dots, z_n]$ is uniformly sampled from the sphere of n -dimension unit ball, where $n \geq 2$. Then for $\frac{1}{n} \leq \delta < 1$ and $\forall i \in [1, n]$, we have*

$$\mathbb{P}(z_i^2 \geq \delta) \leq e^{-\frac{n-1}{2} \cdot \delta + 1}.$$

(Proof in App. F.2). This in turn gives

$$\begin{aligned}
\int_0^1 \min \{1, n \cdot \mathbb{P}(z_1^2 \geq \delta)\} d\delta &\leq \int_0^{\min\{1, \frac{2 \log(n)+2}{n-1}\}} 1 \cdot d\delta + \int_{\min\{1, \frac{2 \log(n)+2}{n-1}\}}^1 n \cdot e^{-\frac{n-1}{2} \cdot \delta + 1} \cdot d\delta \\
&\leq \begin{cases} \frac{2 \log(n)+2}{n-1} - \frac{1}{n-1} e^{-\frac{n-3}{2}} + \frac{2}{n-1} & (n \leq 6) \\ \frac{2}{n-1} & (n \geq 7) \end{cases} \\
&\leq \frac{4 \log(n)}{n-1}
\end{aligned} \tag{14}$$

where Eq. (14) follows from Lemma 4. □

F.2 Proof of Lemma 4

Proof. Due to the symmetry of z_i , we only need to prove the inequality for $i = 1$ case. Let $x = [x_1, \dots, x_n] \sim \mathcal{N}(\mathbf{0}, I_n)$, where I_n is the identity matrix in n dimension. We know that $\frac{x_1^2}{\sum_{i=1}^n x_i^2} \stackrel{d}{=} z_1^2$. Therefore, we have

$$\mathbb{P}(z_1^2 \geq \delta) = \mathbb{P} \left(\frac{x_1^2}{\sum_{j=1}^n x_j^2} \geq \delta \right) = \mathbb{P} \left(\frac{x_1^2}{(\sum_{i=2}^n x_i^2)/(n-1)} \geq \frac{(n-1)\delta}{1-\delta} \right).$$

Note that x_1^2 and $\sum_{i=2}^n x_i^2$ are two independent chi-squared random variables, therefore, we know that $\frac{x_1^2}{(\sum_{i=2}^n x_i^2)/(n-1)} \sim F(1, n-1)$, where F denotes the central F-distribution. Therefore,

$$\begin{aligned}
\mathbb{P} \left(\frac{x_1^2}{(\sum_{i=2}^n x_i^2)/(n-1)} \geq \frac{(n-1)\delta}{1-\delta} \right) &= 1 - I_\delta \left(\frac{1}{2}, \frac{n-1}{2} \right) \\
&= I_{1-\delta} \left(\frac{n-1}{2}, \frac{1}{2} \right) \\
&= \frac{B_{1-\delta} \left(\frac{n-1}{2}, \frac{1}{2} \right)}{B \left(\frac{n-1}{2}, \frac{1}{2} \right)},
\end{aligned} \tag{15}$$

where $I_x(a, b)$ is the regularized incomplete beta function, $B_x(a, b)$ is the incomplete beta function, and $B(a, b)$ is beta function.

For the ease of computation, we take the log of Eq. (15). The numerator gives

$$\begin{aligned}
& \log \left(B_{1-\delta} \left(\frac{n-1}{2}, \frac{1}{2} \right) \right) \\
&= \log \left(\frac{(1-\delta)^{(n-1)/2}}{(n-1)/2} {}_2F_1 \left(\frac{n-1}{2}, \frac{1}{2}; \frac{n+1}{2}; 1-\delta \right) \right) \\
&= \frac{n-1}{2} \log(1-\delta) - \log(n-1) + \log \left({}_2F_1 \left(\frac{n-1}{2}, \frac{1}{2}; \frac{n+1}{2}; 1-\delta \right) \right) + \log(2) \quad , \quad (16)
\end{aligned}$$

where ${}_2F_1(\cdot)$ is the hypergeometric function. Let $(q)_i = \begin{cases} 1 & (i=0) \\ q(q+1)\dots(q+i-1) & (i>0) \end{cases}$, we have

$$\begin{aligned}
& {}_2F_1 \left(\frac{n-1}{2}, \frac{1}{2}; \frac{n+1}{2}; 1-\delta \right) \\
&= \sum_{i=0}^{\infty} \frac{\left(\frac{n-1}{2}\right)_i \left(\frac{1}{2}\right)_i (1-\delta)^i}{\left(\frac{n+1}{2}\right)_i \cdot i!} \\
&\leq \sum_{i=0}^{\infty} \frac{\left(\frac{1}{2}\right)_i (1-\delta)^i}{\cdot i!} \\
&= \delta^{-\frac{1}{2}} \quad (17)
\end{aligned}$$

Substituting it into Eq. (16) gives

$$\log \left(B_{1-\delta} \left(\frac{n-1}{2}, \frac{1}{2} \right) \right) \leq \frac{n-1}{2} \log(1-\delta) - \log(n-1) - \frac{1}{2} \log(\delta) + \log(2) \quad . \quad (18)$$

The log of the denominator of (15) is

$$\begin{aligned}
& \log \left(B \left(\frac{n-1}{2}, \frac{1}{2} \right) \right) \\
&= \log \left(\frac{\Gamma \left(\frac{n-1}{2} \right) \Gamma \left(\frac{1}{2} \right)}{\Gamma \left(\frac{n}{2} \right)} \right) \\
&\geq \log \left(\sqrt{\pi} \cdot \left(\frac{n+1}{2} \right)^{-\frac{1}{2}} \right) \\
&= -\frac{1}{2} \log(n+1) + \frac{1}{2} \log(2) + \frac{1}{2} \log(\pi) \quad . \quad (19)
\end{aligned}$$

where Γ denotes the Gamma function and we use the Gautschi's inequality: $\frac{\Gamma(x+1)}{\Gamma(x+\frac{1}{2})} < (x+1)^{\frac{1}{2}}$ for positive real number x .

Combining Eq. (15), Eq. (18), and Eq. (19) we get

$$\begin{aligned}
& \log \left(\mathbb{P} \left(\frac{x_1^2}{(\sum_{i=2}^n x_i^2)/(n-1)} \geq \frac{(n-1)\delta}{1-\delta} \right) \right) \\
&\leq \frac{n-1}{2} \log(1-\delta) - \log(n-1) + \frac{1}{2} \log(n+1) - \frac{1}{2} \log(\delta) + \frac{1}{2} \log(2/\pi) \\
&\leq \frac{n-1}{2} \log(1-\delta) - \frac{1}{2} \log(n-1) - \frac{1}{2} \log(\delta) + \frac{1}{2} \log(6/\pi) \\
&\leq \frac{n-1}{2} \log(1-\delta) - \frac{1}{2} \log \left(\frac{n-1}{n} \right) + \frac{1}{2} \log(6/\pi) \\
&\leq \frac{n-1}{2} \log(1-\delta) + \frac{1}{2} \log \frac{12}{\pi} \\
&\leq -\frac{n-1}{2} \cdot \delta + 1
\end{aligned}$$

Therefore, we have

$$\mathbb{P}(z_1^2 \geq \delta) \leq e^{-\frac{n-1}{2} \cdot \delta + 1}$$

□

G Proof of Thm. 3

Proof. Let $s_w = c_{in}c_{out}k_wk_h$. Since w_{ij} are symmetric random variables, we know $\mathbb{E}\left(\frac{w_{ij}}{\sigma_w}\right) = 0$. Therefore, we have

$$\text{Var}\left(\frac{w_{ij}}{\sigma_w}\right) = \mathbb{E}\left(\frac{w_{ij}^2}{\sigma_w^2}\right) = \frac{1}{s_w} \cdot \mathbb{E}\left(\frac{\sum_{i=1}^m \sum_{j=1}^n w_{ij}^2}{\sigma_w^2}\right) = \frac{1}{s_w} \cdot \mathbb{E}\left(\frac{\|w\|_F^2}{\sigma_w^2}\right)$$

Note that

$$\begin{aligned} \frac{1}{s_w} \cdot \mathbb{E}\left(\frac{\|w\|_F^2}{\sigma_w^2}\right) &\in \left[\frac{2}{s_w} \cdot \mathbb{E}\left(\frac{\|w\|_F^2}{\|w^{c_{out} \times (c_{in}k_wk_h)}\|_{\text{sp}}^2 + \|w^{c_{in} \times (c_{out}k_wk_h)}\|_{\text{sp}}^2}\right), \right. \\ &\quad \left. \frac{4}{s_w} \cdot \mathbb{E}\left(\frac{\|w\|_F^2}{\|w^{c_{out} \times (c_{in}k_wk_h)}\|_{\text{sp}}^2 + \|w^{c_{in} \times (c_{out}k_wk_h)}\|_{\text{sp}}^2}\right) \right]. \end{aligned}$$

Assume the singular values of $w^{c_{out} \times (c_{in}k_wk_h)}$ are $\sigma_1 \geq \sigma_2 \geq \dots \geq \sigma_{c_{out}}$, and the singular values of $w^{c_{in} \times (c_{out}k_wk_h)}$ are $\sigma'_1 \geq \sigma'_2 \geq \dots \geq \sigma'_{c_{in}}$. We have

$$\begin{aligned} &\frac{4}{s_w} \cdot \mathbb{E}\left(\frac{\|w\|_F^2}{\|w^{c_{out} \times (c_{in}k_wk_h)}\|_{\text{sp}}^2 + \|w^{c_{in} \times (c_{out}k_wk_h)}\|_{\text{sp}}^2}\right) \\ &= \frac{4}{s_w} \cdot \mathbb{E}\left(\frac{1}{2} \cdot \frac{\sum_{i=1}^{c_{out}} \sigma_i^2}{\sigma_1^2} + \frac{1}{2} \cdot \frac{\sum_{i=1}^{c_{in}} \sigma_i'^2}{\sigma_1'^2}\right) \leq \frac{2(c_{out} + c_{in})}{s_w} = \frac{2}{c_{in}k_wk_h + c_{out}k_wk_h}, \end{aligned}$$

which gives the desired upper bound.

As for the lower bound, observe that

$$\begin{aligned} &\frac{2}{s_w} \cdot \mathbb{E}\left(\frac{\|w\|_F^2}{\|w^{c_{out} \times (c_{in}k_wk_h)}\|_{\text{sp}}^2 + \|w^{c_{in} \times (c_{out}k_wk_h)}\|_{\text{sp}}^2}\right) \\ &= \frac{2}{s_w} \cdot \mathbb{E}\left(\frac{1}{\left\|\frac{w^{c_{out} \times (c_{in}k_wk_h)}}{\|w\|_F}\right\|_{\text{sp}}^2 + \left\|\frac{w^{c_{in} \times (c_{out}k_wk_h)}}{\|w\|_F}\right\|_{\text{sp}}^2}\right) \\ &\geq \frac{2}{s_w} \cdot \frac{1}{\mathbb{E}\left(\left\|\frac{w^{c_{out} \times (c_{in}k_wk_h)}}{\|w\|_F}\right\|_{\text{sp}}^2\right) + \mathbb{E}\left(\left\|\frac{w^{c_{in} \times (c_{out}k_wk_h)}}{\|w\|_F}\right\|_{\text{sp}}^2\right)} \end{aligned}$$

Then we can follow the same approach in App. F for bounding $\mathbb{E}\left(\left\|\frac{w^{c_{out} \times (c_{in}k_wk_h)}}{\|w\|_F}\right\|_{\text{sp}}^2\right)$ and $\mathbb{E}\left(\left\|\frac{w^{c_{in} \times (c_{out}k_wk_h)}}{\|w\|_F}\right\|_{\text{sp}}^2\right)$, which gives the desired lower bound. □

H Datasets and Metrics

H.1 Datasets

MNIST [21] We use the training set for our experiments, which contains 60000 images of hand-written digits of shape $28 \times 28 \times 1$. The pixels values are normalized to $[0, 1]$ before feeding to the discriminators.

CIFAR10 [19] We use the training set for our experiments, which contains 50000 images of shape $32 \times 32 \times 3$. The pixels values are normalized to $[-1, 1]$ before feeding to the discriminators.

STL10 [7] We use the unlabeled set for our experiments, which contains 100000 images of shape $96 \times 96 \times 3$. Following [25], we resize the images to $48 \times 48 \times 3$ for training. The pixels values are normalized to $[-1, 1]$ before feeding to the discriminators.

CelebA [24] This dataset contains 202599 images. For each image, we crop the center 128×128 , and resize it to $64 \times 64 \times 3$ for training. The pixels values are normalized to $[-1, 1]$ before feeding to the discriminators.

ImageNet (ILSVRC2012) [33] The dataset contains 1281167 images. Following [25], for each images, we crop the central square of the images according to $\min(\text{width}, \text{height})$, and then reshape it to $128 \times 128 \times 3$ for training. The pixels values are normalized to $[-1, 1]$ before feeding to the discriminators.

H.2 Metrics

Inception score [34] Following [25], we use 50000 generated images and split them into 10 sets for computing the score.

FID [15] Following [25], we use 5000 real images and 10000 generated images for computing the score.

I Gradient Explosion and Vanishing in GANs

I.1 Results

To illustrate that gradient explosion and vanishing are closely related to the instability in GANs, we trained a WGAN [13] on the CIFAR10 dataset with different hyperparameters leading to stable training, exploding gradients, and vanishing gradients over 40,000 training iterations (more experimental details in App. I.2). Fig. 10 shows the resulting inception scores for each of these runs, and Fig. 11 shows the corresponding magnitudes of the gradients over the course of training. Note that the stable run has improved sample quality and stable gradients throughout training. This phenomenon has also been observed in prior literature [1, 5]. We will demonstrate that by controlling these gradients, SN (and SN_w in particular) is able to achieve more stable training and better sample quality.

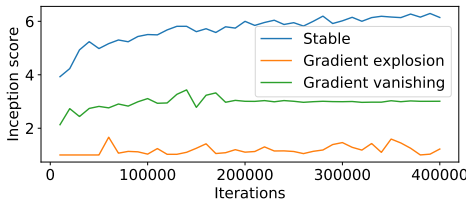


Figure 10: Inception score over the course of training. The “gradient vanishing” inception score plateaus as training is stalled.

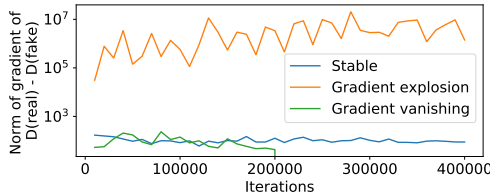


Figure 11: Norm of gradient with respect to parameters during training. The vanishing gradient collapses after 200k iterations.

$z \in \mathbb{R}^{128} \sim \mathcal{N}(0, I)$
Fully connected ($M_g \times M_g \times 512$). BN. ReLU.
Deconvolution ($c = 256, k = 4, s = 2$). BN. ReLU.
Deconvolution ($c = 128, k = 4, s = 2$). BN. ReLU.
Deconvolution ($c = 64, k = 4, s = 2$). BN. ReLU.
Deconvolution ($c = 3, k = 3, s = 1$). Tanh.

Table 3: Generator network architectures for CIFAR10, STL10, and CelebA experiments (from [25]). For CIFAR10, $M_g = 4$. For STL10, $M_g = 6$. For CelebA, $M_g = 8$. BN stands for batch normalization. c stands for number of channels. k stands for kernel size. s stands for stride.

$x \in \mathbb{R}^{M \times M \times 3}$
Convolution ($c = 64, k = 3, s = 1$). Leaky ReLU (0.1).
Convolution ($c = 64, k = 4, s = 2$). Leaky ReLU (0.1).
Convolution ($c = 128, k = 3, s = 1$). Leaky ReLU (0.1).
Convolution ($c = 128, k = 4, s = 2$). Leaky ReLU (0.1).
Convolution ($c = 256, k = 3, s = 1$). Leaky ReLU (0.1).
Convolution ($c = 256, k = 4, s = 2$). Leaky ReLU (0.1).
Convolution ($c = 512, k = 3, s = 1$). Leaky ReLU (0.1).
Fully connected (1).

Table 4: Discriminator network architectures for CIFAR10, STL10, and CelebA experiments (from [25]). For CIFAR10, $M = 32$. For STL10, $M = 48$. For CelebA, $M = 64$. c stands for number of channels. k stands for kernel size. s stands for stride.

I.2 Experimental Details

The network architectures are shown in Tables 3 and 4. The dataset is CIFAR10. All experiments are run for 400k iterations. Batch size is 64. The optimizer is Adam. Let λ be the WGAN’s gradient penalty weight [13]. For the stable run, $\alpha_g = 0.0001, \alpha_d = 0.0002, \beta_1 = 0.5, \beta_2 = 0.999, \lambda = 10, n_{dis} = 1$. For the gradient explosion run, $\alpha_g = 0.001, \alpha_d = 0.001, \beta_1 = 0.5, \beta_2 = 0.999, \lambda = 10, n_{dis} = 1$. For the gradient vanishing run, $\alpha_g = 0.001, \alpha_d = 0.001, \beta_1 = 0.5, \beta_2 = 0.999, \lambda = 50, n_{dis} = 1$, and the activation functions in the discriminator are changed from leaky ReLU to ReLU.

J Experimental Details and Additional Results on Gradient Norms

J.1 Experimental Details

For the MNIST experiment, the network architectures are shown in Tables 5 and 6. All experiments are run for 100 epochs. Batch size is 64. The optimizer is Adam. $\alpha_g = 0.001, \alpha_d = 0.001, \beta_1 = 0.5, \beta_2 = 0.999, n_{dis} = 1$.

For the CIFAR10 experiment, the network architectures are shown in Tables 3 and 4. All experiments are run for 400k iterations. Batch size is 64. The optimizer is Adam. $\alpha_g = 0.0001, \alpha_d = 0.0001, \beta_1 = 0.5, \beta_2 = 0.999, n_{dis} = 1$.

Let λ be the WGAN’s gradient penalty weight [13]. For the runs without SN, $\lambda = 10$. For the runs with SN, we use the strict SN implementation [8] in order to verifying the theoretical results (the popular SN implementation [25] only gives a loose bound on the actual spectral norm of layers, see § 4). Since it already ensures that the Lipschitz constant of the discriminator is no more than 1, we discard the gradient penalty loss from training.

For all the results, the gradient norm only considers the weights and excludes the biases (if exist), so as to be consistent with the theoretical analysis.

$z \in \mathbb{R}^{100} \sim \text{Uniform}(-1, 1)$
Fully connected ($7 \times 7 \times 128$). Leaky ReLU (0.2). BN.
Deconvolution ($c = 64, k = 5, s = 2$). Leaky ReLU (0.2). BN.
Deconvolution ($c = 1, k = 5, s = 2$). Sigmoid.

Table 5: Generator network architectures for MNIST experiments. BN stands for batch normalization. c stands for number of channels. k stands for kernel size. s stands for stride.

$x \in \mathbb{R}^{28 \times 28 \times 1}$
Convolution ($c = 64, k = 5, s = 2$, no bias). Leaky ReLU (0.2).
Convolution ($c = 128, k = 5, s = 2$, no bias). Leaky ReLU (0.2).
Convolution ($c = 256, k = 5, s = 2$, no bias). Leaky ReLU (0.2).
Fully connected (1, no bias).

Table 6: Discriminator network architectures for MNIST experiments. c stands for number of channels. k stands for kernel size. s stands for stride.

J.2 Additional Results

Figs. 12 and 13 show the gradient norms of each discriminator layer in MNIST and CIFAR10. Despite the difference on the network architecture and dataset, we see the similar phenomenon: when training without SN, some layers have extremely large gradient norms, which causes the overall gradient norm to be large; when training with SN, the gradient norms are much smaller and are similar across different layers.

K Experimental Details and Additional Results for Confirming Eq. (3)

K.1 Experimental Details

For the MNIST experiment, the network architectures are shown in Tables 5 and 6. All experiments are run for 100 epochs. Batch size is 64. The optimizer is Adam. $\alpha_g = 0.001, \alpha_d = 0.001, \beta_1 = 0.5, \beta_2 = 0.999, n_{dis} = 1$. We use WGAN loss with the strict SN implementation [8]. Since it already ensures that the Lipschitz constant of the discriminator is no more than 1, we discard the gradient penalty loss from training. The random scaling are selected in a way the geometric mean of spectral norms of all layers equals 1.

For the CIFAR10 and STL10 experiments, the network architectures are shown in Tables 3 and 4. All experiments are run for 400k iterations. Batch size is 64. The optimizer is Adam. $\alpha_g = 0.0001, \alpha_d = 0.0001, \beta_1 = 0.5, \beta_2 = 0.999, n_{dis} = 1$. We use hinge loss [25] with the strict SN implementation [8]. The random scaling are selected in a way the geometric mean of spectral norms of all layers equals 1.75, which avoids the gradient vanishing problem as seen in § 4.

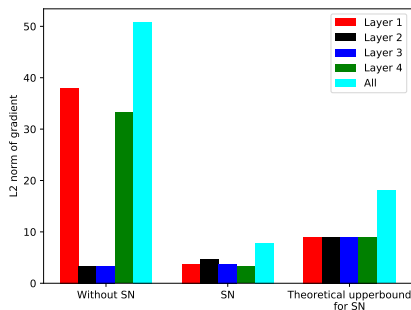


Figure 12: Gradient norms of each discriminator layer in MNIST at epoch 50.

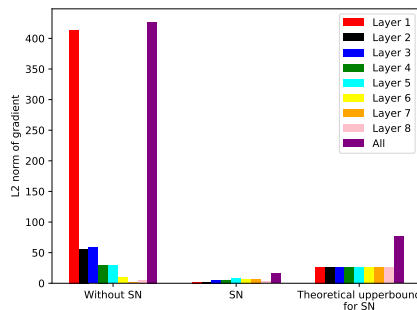


Figure 13: Gradient norms of each discriminator layer in CIFAR10 at iteration 10000.

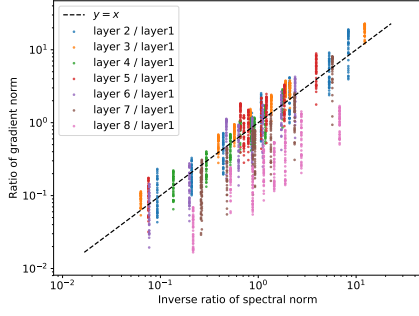


Figure 14: Ratio of gradient norm v.s. inverse ratio of spectral norm in CIFAR10.

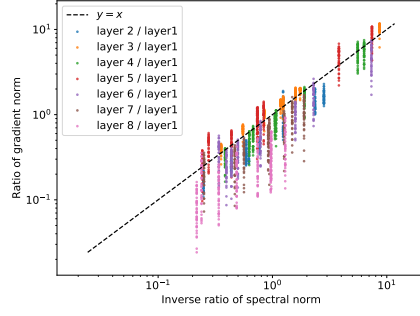


Figure 15: Ratio of gradient norm v.s. inverse ratio of spectral norm in STL10.

K.2 Additional Results

Figs. 14 and 15 show the ratios of the gradient norms at each layer and the inverse ratios of the spectral norms in CIFAR10 and STL10. Generally, we see that the most of the points are near the diagonal line, which means that the assumption in Eq. (3) is reasonably true in practice. However, we note that the last layer (layer 8) somehow has slightly smaller gradient, as the points of “layer 8 / layer 1” are slightly lower than the diagonal line. This could result from the fact that layer 8 is a fully connected layer whereas all other layers are convolutional layers. We defer the more detailed analysis of this phenomenon to future work.

L Experimental Details and Additional Results on Vanishing Gradient

L.1 Experimental Details

The network architectures are shown in Tables 3 and 4. The dataset is CIFAR10. All experiments are run for 400k iterations. Batch size is 64. The optimizer is Adam. $\alpha_g = 0.0001$, $\alpha_d = 0.0001$, $\beta_1 = 0.5$, $\beta_2 = 0.999$, $n_{dis} = 1$. We use hinge loss [25].

L.2 Parameter Variance With and Without SN

Figs. 16 and 17 show the parameter variance of each layer without and with SN. Note that Fig. 17 is just collecting the empirical lines in Fig. 3 for the ease of comparison here. Figs. 18 and 19 show the gradient norm and inception score.

We can see that when training with SN, the parameter variance is stable throughout training (Fig. 17), and the magnitude of gradient is also stable (Fig. 18). However, when training without SN, the parameter variance tends to increase throughout training (Fig. 16), which causes a quick decrease in the magnitude of gradient in the beginning of training (Fig. 18) because of the saturation of hinge loss (§ 4). Because SN promotes the stability of the variance and gradient throughout training, we see that SN improves the sample quality significantly (Fig. 19).

L.3 Comparing Two Variants Spectral Norms

Figs. 20 and 21 show the ratio between two versions of spectral norm [25, 8] throughout the training of the popular SN [25] and the strict SN [8]. $\|Conv\|_{sp}$ denotes the spectral norm of the expanded matrix $\|\tilde{w}\|_{sp}$ used in [8]. $\|w\|_{sp}$ denotes the spectral norm of reshaped matrix $\|\hat{w}\|_{sp}$ used in [25]. The theoretical lower and upper bound are calculated according to Corollary 1 in [38]. We can see that no matter in which architecture, $\|\tilde{w}\|_{sp}$ is usually strictly larger than $\|\hat{w}\|_{sp}$. Note that the reason why in some cases the ratio exceeds the upper bound in Fig. 20 is because the spectral norms are calculated using power iteration [25, 8] which has approximation error.

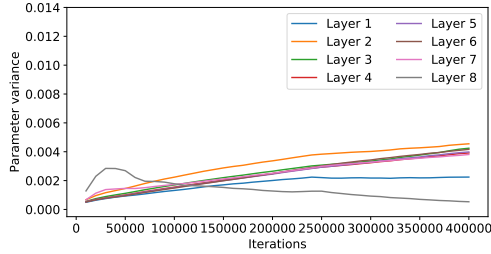


Figure 16: Parameter variance without SN in CIFAR10.

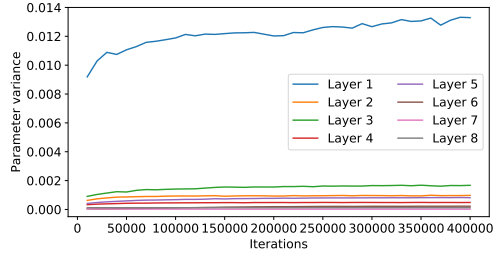


Figure 17: Parameter variance with SN in CIFAR10.

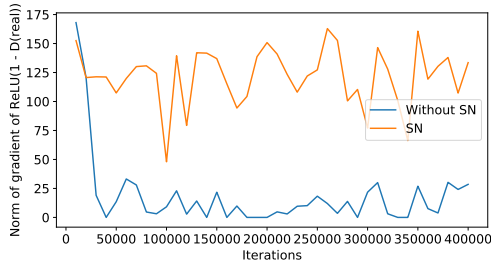


Figure 18: Gradient norm with and without SN in CIFAR10.

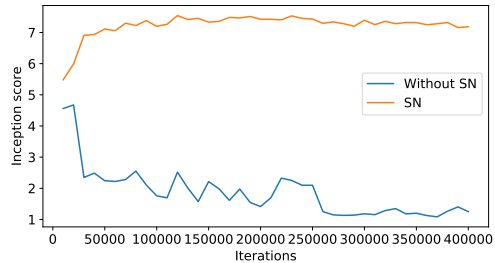


Figure 19: Inception score with and without SN in CIFAR10.

L.4 Parameter Variance of Scaled SN

Figure Fig. 22 shows the parameter variance of scaled SN for both SN versions [25, 8]. We can see that when $\text{scale}=1.75$, the product of parameter variances for SN_{conv} [8] is similar to the one of SN_w [25]. Moreover, by comparing Fig. 22 and Fig. 6 we can see that when the products of variances of two SN variants are similar, the sample quality is also similar. This confirms the intuition from LeCun initialization [20] that the magnitude of variance plays an important role on the performance of neural network, and it should not be too large nor too small.

M Details on SN Variants

In Appendix E of [25], a variant of SN is introduced. Instead of strictly setting the spectral norm of each layer, the idea of this approach is to release the constraint by multiplying each spectral normalized weights with a trainable parameter γ . However, this would make the gradient of discriminator arbitrarily large, which violates the original motivation of SN. Therefore, the approach incorporates gradient penalty [13] for setting the Lipschitz constant of discriminator to 1. The gradient penalty weights are set to 10 in all experiments.

However, from the description in [25], it is unclear if all layers have the same or separated γ . Therefore, we try both versions in our experiments. “Same γ ” denotes that version where all layers share the same γ . “Diff. γ ” denotes the version where each layer has a separate γ .

N Experimental Details and Additional Results on CIFAR10

N.1 Experimental Details

The network architectures are shown in Tables 3 and 4. All experiments are run for 400k iterations. Batch size is 64. The optimizer is Adam. We use the five hyper-parameter settings listed in Table 7. We use hinge loss with the popular SN implementation [25].

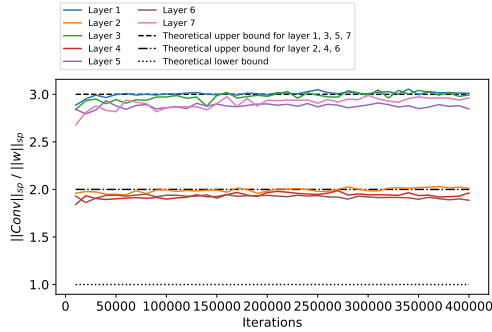


Figure 20: The ratio of two spectral norms throughout the training of the popular SN [25] in CIFAR10.

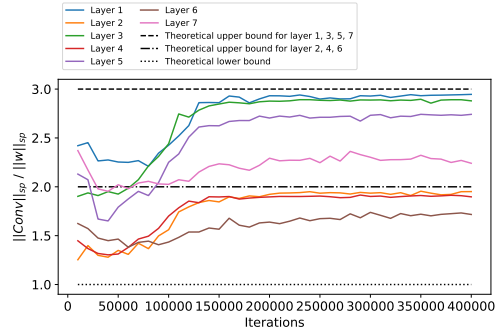


Figure 21: The ratio of two spectral norms throughout the training of the strict SN [8] in CIFAR10.

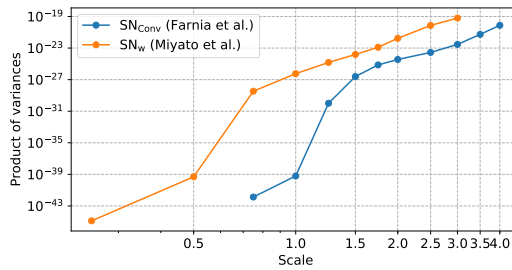


Figure 22: The parameter variance of scaled SN in CIFAR10.

N.2 FID Plot

Fig. 23 shows the FID score in CIFAR10 dataset. We can see that BSN has the best performance in all 5 hyper-parameter settings.

N.3 Training Curves

From § 5.1 we can see that SN (no γ) and BSN generally have the best performance. Therefore, in this section, we focus on comparing these two algorithms with the training curves. Figs. 7 and 24 to 32 show the inception score and FID of these two algorithms during training. Generally, we see that BSN converges slower than SN *at the beginning of training*. However, as training proceeds, the sample quality of SN often drops (e.g. Figs. 7 and 24 to 30), whereas the sample quality of BSN always increases and then stabilizes at the high level. In most cases, BSN not only outperforms SN at the end of training, but also outperforms the peak sample quality of SN during training (e.g. Figs. 7 and 24 to 30). From these results, we can conclude that BSN improves both the sample quality and training stability over SN.

α_g	α_d	β_1	β_2	n_{dis}
0.0001	0.0001	0.5	0.9	5
0.0001	0.0001	0.5	0.999	1
0.0002	0.0002	0.5	0.999	1
0.0001	0.0002	0.5	0.999	1
0.0002	0.0001	0.5	0.999	1

Table 7: Hyper-parameters tested in CIFAR10 and STL10 experiments. The first three settings are from [25, 13, 40, 32]. α_g and α_d : learning rates for generator and discriminator. β_1, β_2 : momentum parameters in Adam. n_{dis} : number of discriminator updates per generator update.

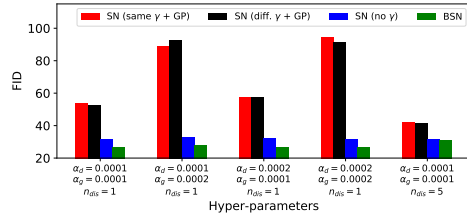


Figure 23: FID in CIFAR10. The results are averaged over 5 random seeds.

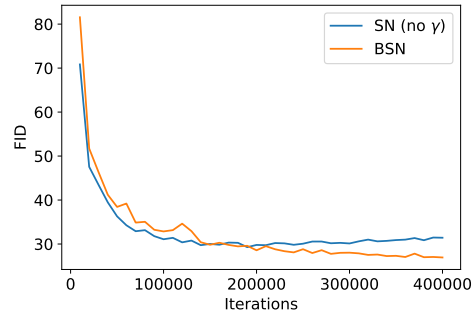


Figure 24: FID in CIFAR10. The results are averaged over 5 random seeds. The hyper-parameters are: $\alpha_g = 0.0001$, $\alpha_d = 0.0001$, $n_{dis} = 1$.

N.4 Generated Images

Figs. 33 to 36 show the generated images from the run with the best inception score for each algorithm.

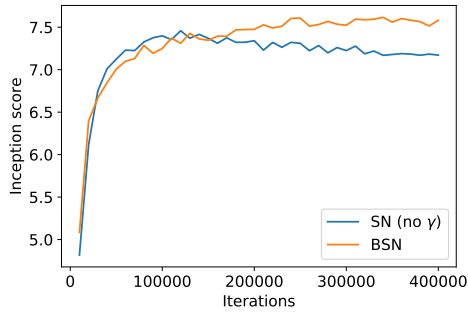


Figure 25: Inception score in CIFAR10. The results are averaged over 5 random seeds. The hyper-parameters are: $\alpha_g = 0.0001$, $\alpha_d = 0.0002$, $n_{dis} = 1$.

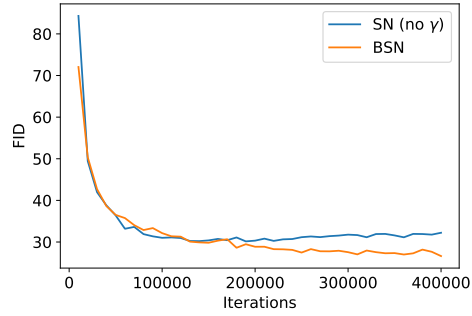


Figure 26: FID in CIFAR10. The results are averaged over 5 random seeds. The hyper-parameters are: $\alpha_g = 0.0001$, $\alpha_d = 0.0002$, $n_{dis} = 1$.

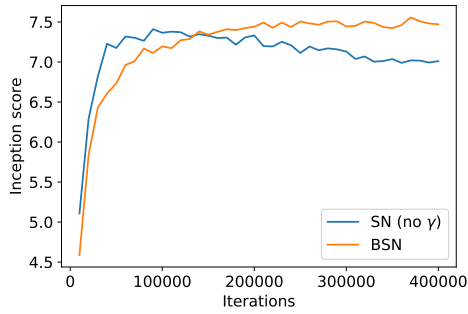


Figure 27: Inception score in CIFAR10. The results are averaged over 5 random seeds. The hyper-parameters are: $\alpha_g = 0.0002$, $\alpha_d = 0.0001$, $n_{dis} = 1$.

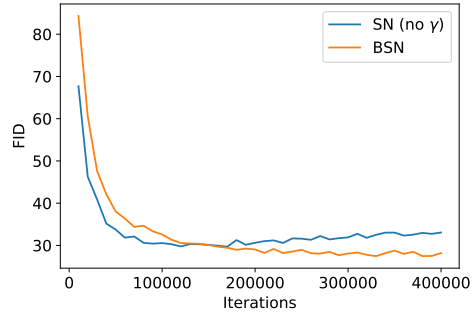


Figure 28: FID in CIFAR10. The results are averaged over 5 random seeds. The hyper-parameters are: $\alpha_g = 0.0002$, $\alpha_d = 0.0001$, $n_{dis} = 1$.

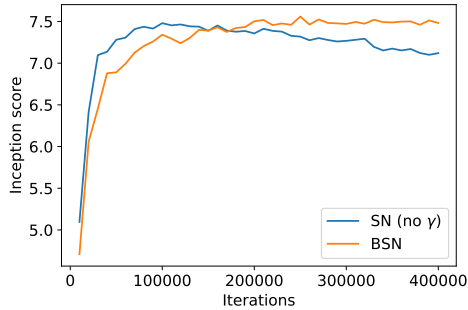


Figure 29: Inception score in CIFAR10. The results are averaged over 5 random seeds. The hyper-parameters are: $\alpha_g = 0.0002$, $\alpha_d = 0.0002$, $n_{dis} = 1$.

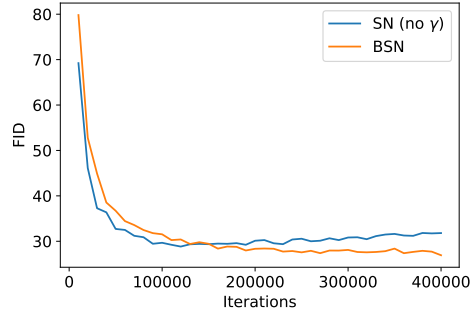


Figure 30: FID in CIFAR10. The results are averaged over 5 random seeds. The hyper-parameters are: $\alpha_g = 0.0002$, $\alpha_d = 0.0002$, $n_{dis} = 1$.

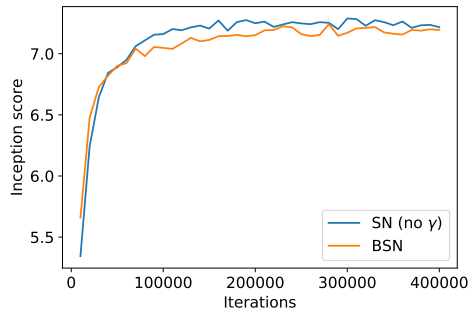


Figure 31: Inception score in CIFAR10. The results are averaged over 5 random seeds. The hyper-parameters are: $\alpha_g = 0.0001$, $\alpha_d = 0.0001$, $n_{dis} = 5$.

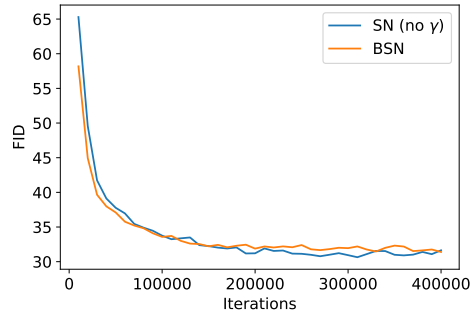


Figure 32: FID in CIFAR10. The results are averaged over 5 random seeds. The hyper-parameters are: $\alpha_g = 0.0001$, $\alpha_d = 0.0001$, $n_{dis} = 5$.

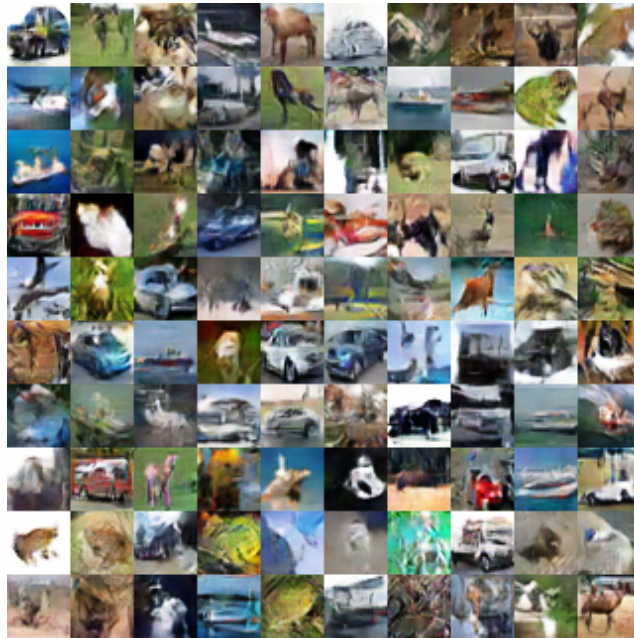


Figure 33: Generated samples from the best run of SN (same γ) in CIFAR10. The hyper-parameters are: $\alpha_g = 0.0001$, $\alpha_d = 0.0001$, $n_{dis} = 5$. Inception score is 6.64. FID is 41.01.

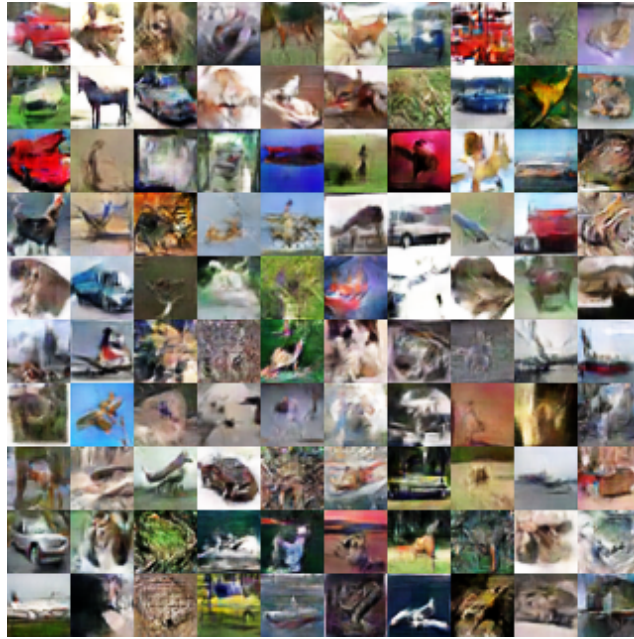


Figure 34: Generated samples from the best run of SN (diff. γ) in CIFAR10. The hyper-parameters are: $\alpha_g = 0.0001$, $\alpha_d = 0.0001$, $n_{dis} = 5$. Inception score is 6.55. FID is 41.18.



Figure 35: Generated samples from the best run of SN (no γ) in CIFAR10. The hyper-parameters are: $\alpha_g = 0.0001$, $\alpha_d = 0.0002$, $n_{dis} = 1$. Inception score is 7.56. FID is 28.64.

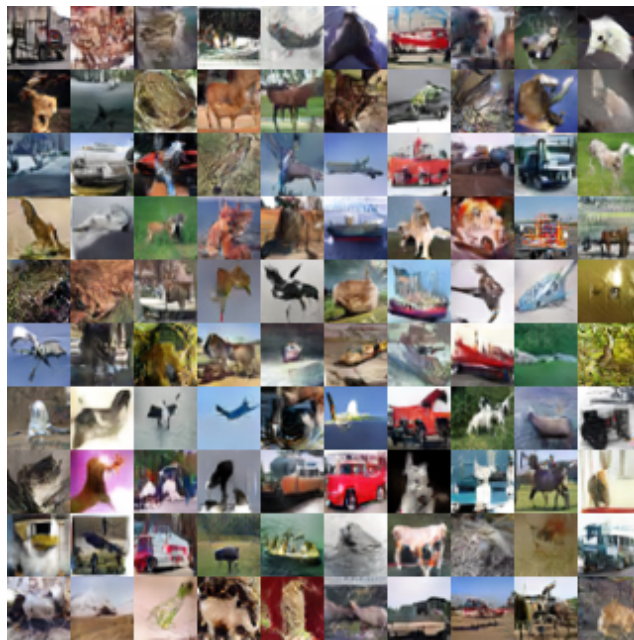


Figure 36: Generated samples from the best run of BSN in CIFAR10. The hyper-parameters are: $\alpha_g = 0.0001$, $\alpha_d = 0.0002$, $n_{dis} = 1$. Inception score is 7.70. FID is 25.96.

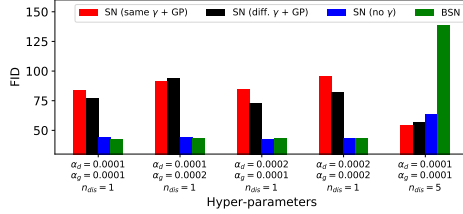


Figure 37: FID in STL10. The results are averaged over 5 random seeds.

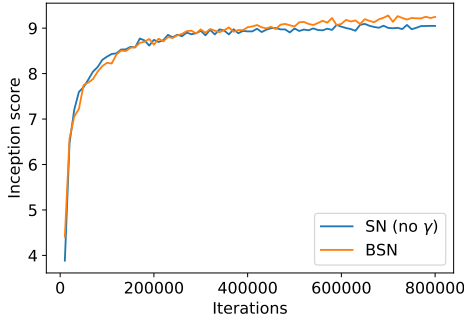


Figure 38: Inception score in STL10. The results are averaged over 5 random seeds. The hyper-parameters are: $\alpha_g = 0.0001$, $\alpha_d = 0.0001$, $n_{dis} = 1$.

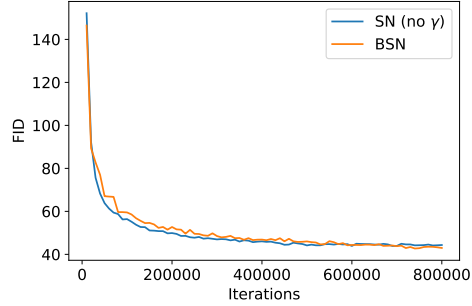


Figure 39: FID in STL10. The results are averaged over 5 random seeds. The hyper-parameters are: $\alpha_g = 0.0001$, $\alpha_d = 0.0001$, $n_{dis} = 1$.

O Experimental Details and Additional Results on STL10

O.1 Experimental Details

The network architectures are shown in Tables 3 and 4. Batch size is 64. The optimizer is Adam. We use the five hyper-parameter settings listed in Table 7. We use hinge loss with the popular SN implementation [25].

SN (no γ) and BSN under $n_{dis} = 1$ settings are run for 800k iterations as we observe that they need longer time to converge. All other experiments are run for 400k iterations.

O.2 FID Plot

Fig. 37 shows the FID score in STL10 dataset. We can see that BSN has the best or competitive performance in most of the hyper-parameter settings. Again, the only exception is $n_{dis} = 5$ setting.

O.3 Training Curves

From § 5.1 we can see that SN (no γ) and BSN generally have the best performance. Therefore, in this section, we focus on comparing these two algorithms with the training curves. Figs. 38 to 47 show the inception score and FID of these two algorithms during training. Generally, we see that BSN converges slower than SN *at the beginning of training*. However, as training proceeds, BSN finally has better metrics in most cases. Note that unlike CIFAR10, SN seems to be more stable in STL10 as its sample quality does not drop in most hyper-parameters. But the key conclusion is the same: in most cases, BSN not only outperforms SN at the end of training, but also outperforms the peak sample quality of SN during training (e.g. Figs. 38 to 45). The only exception is the $n_{dis} = 5$ setting, where both SN and BSN has instability issue: the sample quality first improves and then significantly drops. The problem with BSN seems to be severer. We discussed about this problem in § 5.1.

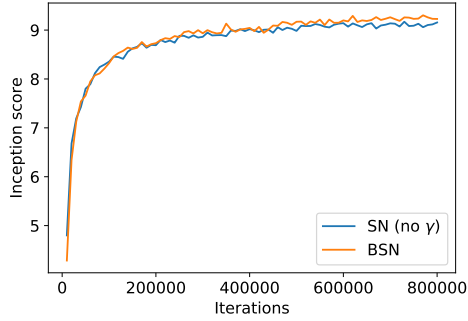


Figure 40: Inception score in STL10. The results are averaged over 5 random seeds. The hyper-parameters are: $\alpha_g = 0.0001$, $\alpha_d = 0.0002$, $n_{dis} = 1$.

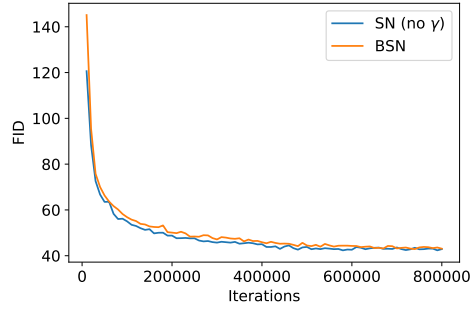


Figure 41: FID in STL10. The results are averaged over 5 random seeds. The hyper-parameters are: $\alpha_g = 0.0001$, $\alpha_d = 0.0002$, $n_{dis} = 1$.

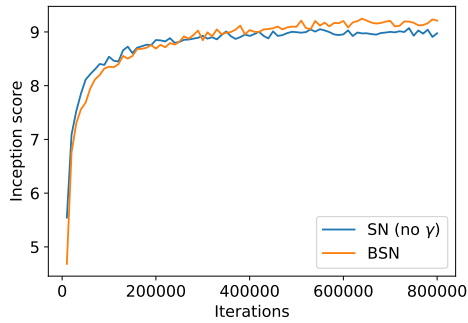


Figure 42: Inception score in STL10. The results are averaged over 5 random seeds. The hyper-parameters are: $\alpha_g = 0.0002$, $\alpha_d = 0.0001$, $n_{dis} = 1$.

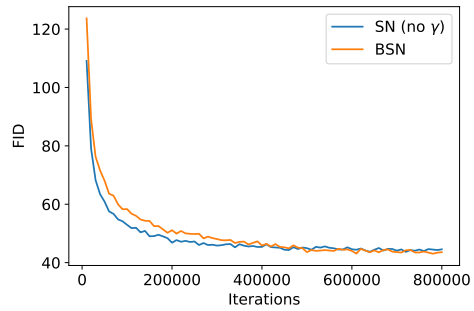


Figure 43: FID in STL10. The results are averaged over 5 random seeds. The hyper-parameters are: $\alpha_g = 0.0002$, $\alpha_d = 0.0001$, $n_{dis} = 1$.

O.4 Generated Images

Figs. 48 to 51 show the generated images from the run with the best inception score for each algorithm.

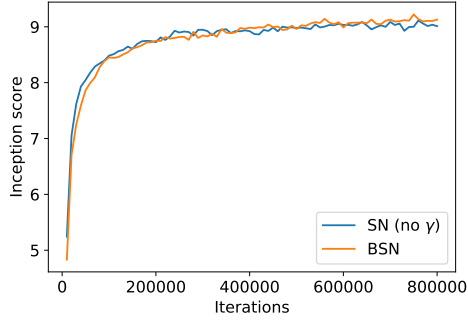


Figure 44: Inception score in STL10. The results are averaged over 5 random seeds. The hyper-parameters are: $\alpha_g = 0.0002$, $\alpha_d = 0.0002$, $n_{dis} = 1$.

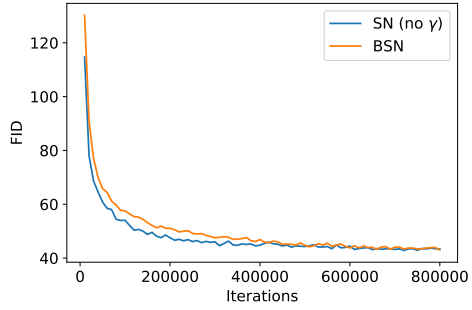


Figure 45: FID in STL10. The results are averaged over 5 random seeds. The hyper-parameters are: $\alpha_g = 0.0002$, $\alpha_d = 0.0002$, $n_{dis} = 1$.

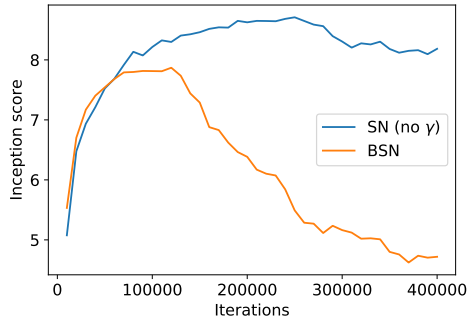


Figure 46: Inception score in STL10. The results are averaged over 5 random seeds. The hyper-parameters are: $\alpha_g = 0.0001$, $\alpha_d = 0.0001$, $n_{dis} = 5$.

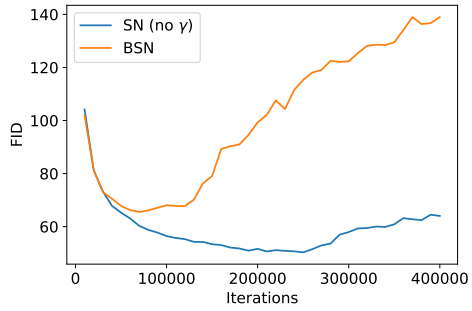


Figure 47: FID in STL10. The results are averaged over 5 random seeds. The hyper-parameters are: $\alpha_g = 0.0001$, $\alpha_d = 0.0001$, $n_{dis} = 5$.



Figure 48: Generated samples from the best run of SN (same γ) in STL10. The hyper-parameters are: $\alpha_g = 0.0001$, $\alpha_d = 0.0001$, $n_{dis} = 5$. Inception score is 8.96. FID is 53.94.

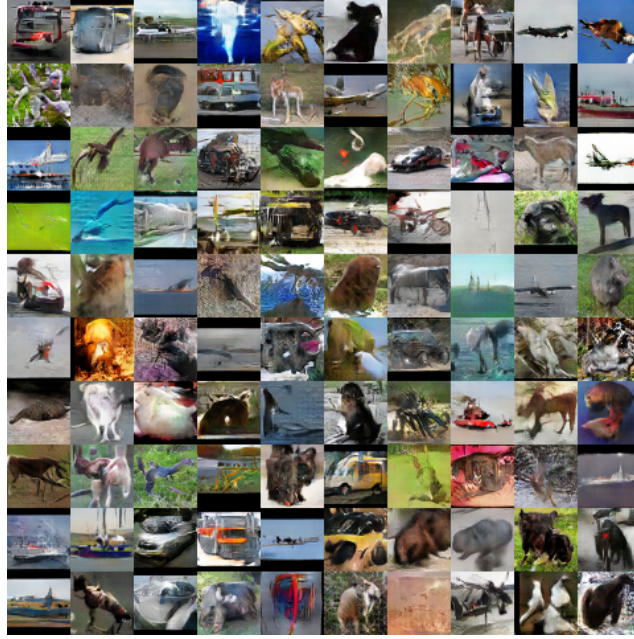


Figure 49: Generated samples from the best run of SN (diff. γ) in STL10. The hyper-parameters are: $\alpha_g = 0.0001$, $\alpha_d = 0.0001$, $n_{dis} = 5$. Inception score is 8.88. FID is 56.14.

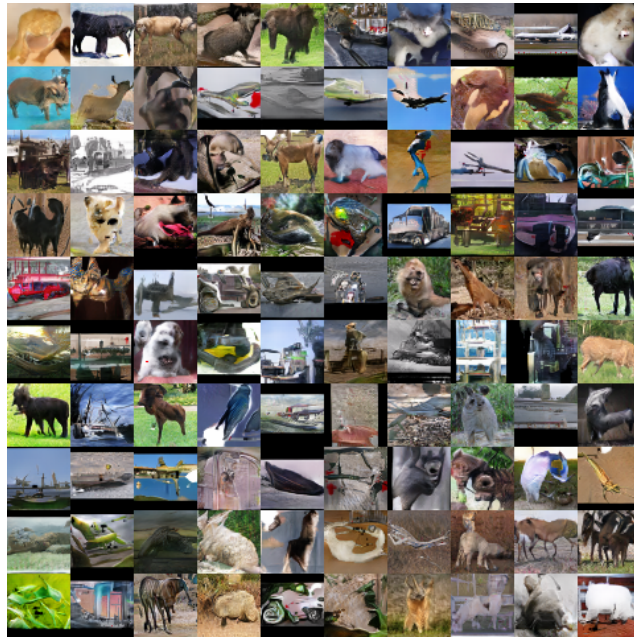


Figure 50: Generated samples from the best run of SN (no γ) in STL10. The hyper-parameters are: $\alpha_g = 0.0001$, $\alpha_d = 0.0002$, $n_{dis} = 1$. Inception score is 9.26. FID is 44.38.

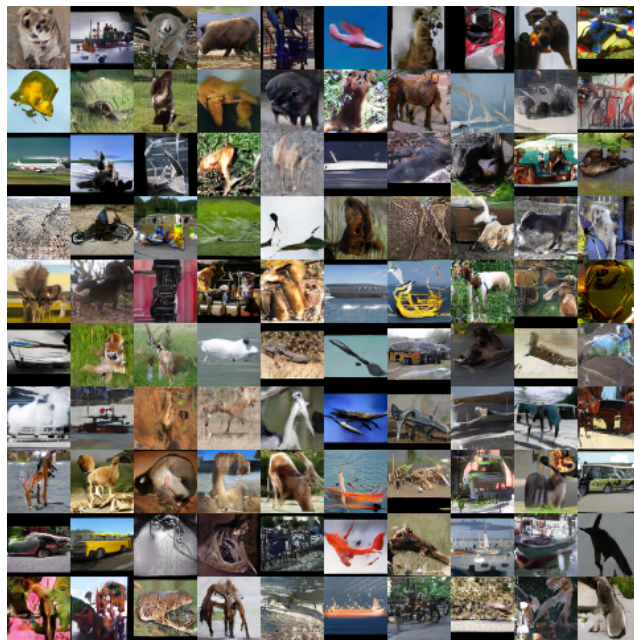


Figure 51: Generated samples from the best run of BSN in STL10. The hyper-parameters are: $\alpha_g = 0.0001$, $\alpha_d = 0.0002$, $n_{dis} = 1$. Inception score is 9.46. FID is 42.78.

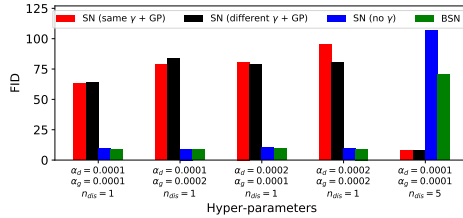


Figure 52: FID in CelebA. The results are averaged over 5 random seeds.

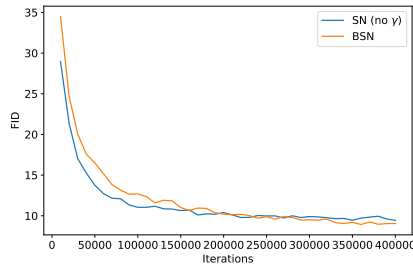


Figure 53: FID in CelebA. The results are averaged over 5 random seeds. The hyper-parameters are: $\alpha_g = 0.0001$, $\alpha_d = 0.0001$, $n_{dis} = 1$.

P Experimental Details and Additional Results on CelebA

P.1 Experimental Details

The network architectures are shown in Tables 3 and 4. All experiments are run for 400k iterations. Batch size is 64. The optimizer is Adam. We use the five hyper-parameter settings listed in Table 7. We use hinge loss with the popular SN implementation [25].

P.2 FID Plot

Fig. 52 shows the FID score in CelebA dataset. We can see that BSN outperforms the standard SN in all 5 hyper-parameter settings.

P.3 Training Curves

From § 5.1 we can see that SN (no γ) and BSN generally have the best performance. Therefore, in this section, we focus on comparing these two algorithms with the training curves. Figs. 53 to 57 show the FID of these two algorithms during training. Generally, we see that BSN converges slower than SN *at the beginning of training*. However, as training proceeds, BSN finally has better metrics in all cases. Note that unlike CIFAR10, SN seems to be more stable in CelebA as its sample quality does not drop in most hyper-parameters. But the key conclusion is the same: in most cases, BSN not only outperforms SN at the end of training, but also outperforms the peak sample quality of SN during training (e.g. Figs. 53 to 56). The only exception is the $n_{dis} = 5$ setting, where both SN and BSN has instability issue: the sample quality first improves and then significantly drops. But even in this case, BSN has better final performance than the standard SN.

P.4 Generated Images

Figs. 58 to 61 show the generated images from the run with the best FID for each algorithm.

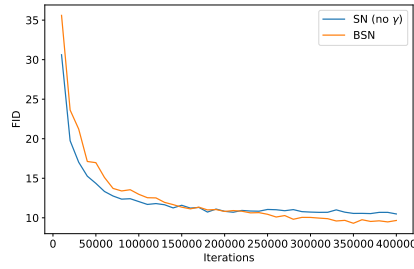


Figure 54: FID in CelebA. The results are averaged over 5 random seeds. The hyper-parameters are: $\alpha_g = 0.0001$, $\alpha_d = 0.0002$, $n_{dis} = 1$.

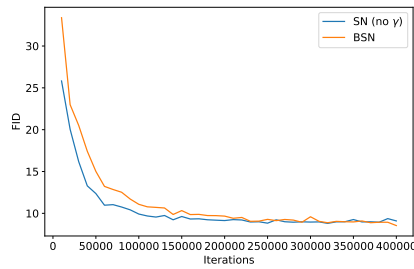


Figure 55: FID in CelebA. The results are averaged over 5 random seeds. The hyper-parameters are: $\alpha_g = 0.0002$, $\alpha_d = 0.0001$, $n_{dis} = 1$.

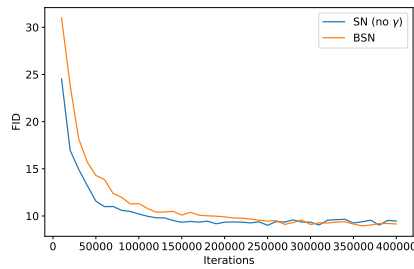


Figure 56: FID in CelebA. The results are averaged over 5 random seeds. The hyper-parameters are: $\alpha_g = 0.0002$, $\alpha_d = 0.0002$, $n_{dis} = 1$.

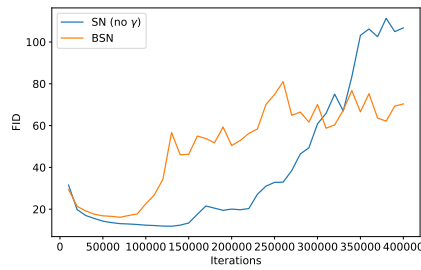


Figure 57: FID in CelebA. The results are averaged over 5 random seeds. The hyper-parameters are: $\alpha_g = 0.0001$, $\alpha_d = 0.0001$, $n_{dis} = 5$.



Figure 58: Generated samples from the best run of SN (same γ) in CelebA. The hyper-parameters are: $\alpha_g = 0.0001$, $\alpha_d = 0.0001$, $n_{dis} = 5$. FID is 7.40.

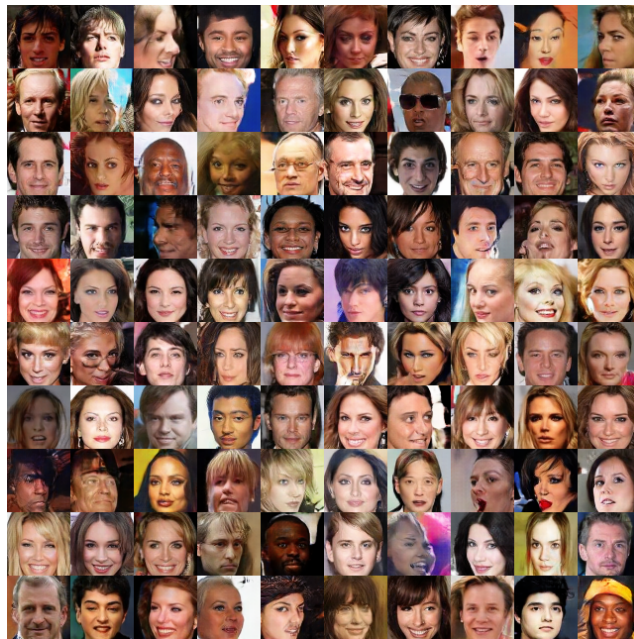


Figure 59: Generated samples from the best run of SN (diff. γ) in CelebA. The hyper-parameters are: $\alpha_g = 0.0001$, $\alpha_d = 0.0001$, $n_{dis} = 5$. FID is 7.29.

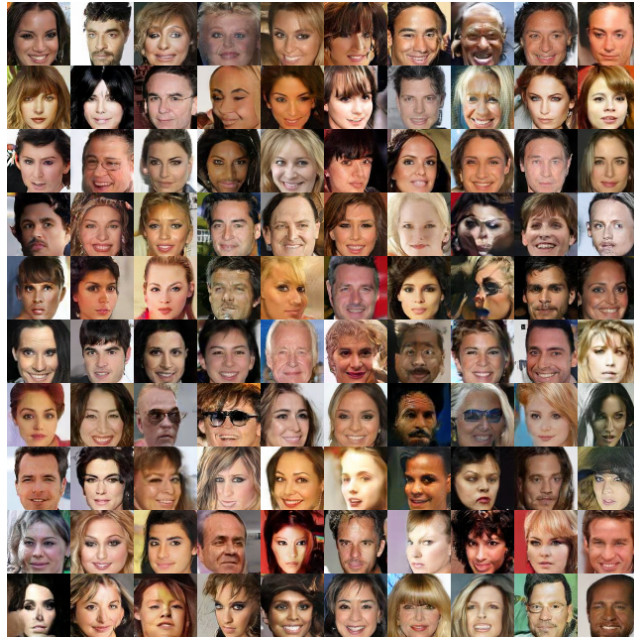


Figure 60: Generated samples from the best run of SN (no γ) in CelebA. The hyper-parameters are: $\alpha_g = 0.0002$, $\alpha_d = 0.0001$, $n_{dis} = 1$. FID is 8.34.



Figure 61: Generated samples from the best run of BSN in CelebA. The hyper-parameters are: $\alpha_g = 0.0002$, $\alpha_d = 0.0001$, $n_{dis} = 1$. FID is 8.06.

$z \in \mathbb{R}^{128} \sim \mathcal{N}(0, I)$
Fully connected ($4 \times 4 \times 1024$).
ResNet-up ($c = 1024$).
ResNet-up ($c = 512$).
ResNet-up ($c = 256$).
ResNet-up ($c = 128$).
ResNet-up ($c = 64$).
BN. ReLU. Convolution ($c = 3, k = 3, s = 1$). Tanh

Table 8: Generator network architectures for ILSVRC2012 experiments (from [25]). BN stands for batch normalization. c stands for number of channels. k stands for kernel size. s stands for stride.

Direct connection
BN. ReLU. Unpooling(2). Convolution ($k = 3, s = 1$).
BN. ReLU. Convolution ($k = 3, s = 1$).
Shortcut connection
Unpooling(2). Convolution ($k = 1, s = 1$).

Table 9: ResNet-up network architectures for ILSVRC2012 experiments (from [25]). BN stands for batch normalization. k stands for kernel size. s stands for stride.

Q Experimental Details and Additional Results on ILSVRC2012

Q.1 Experimental Details

The network architectures are shown in Tables 8 to 13. All experiments are run for 500k iterations. Discriminator batch size is 16. Generator batch size is 32. The optimizer is Adam. $\alpha_g = 0.002, \alpha_d = 0.002, \beta_1 = 0.0, \beta_2 = 0.9, n_{dis} = 5$ We use hinge loss with the popular SN implementation [25].

Q.2 Training Curves

Figs. 62 and 63 show the inception score and FID of SN and BSN during training.

For SN, we can see that the runs with scale=1.0/1.2/1.4 have similar performance throughout training. When scale=1.6, the performance is much worse.

For BSN, the runs with scale=1.2/1.4 perform better than SN runs throughout the training. When scale=1.6, BSN has similar performance as SN at the early stage of training, and is slightly better at the end. When scale=1.0, the performance is very bad as there is gradient vanishing problem.

Q.3 Generated Images

Figs. 64 to 71 show the generated images from the run with the best inception score for SN and BSN with different scale parameters.

$x \in \mathbb{R}^{128 \times 128 \times 3}$
ResNet-first ($c = 64$).
ResNet-down ($c = 128$).
ResNet-down ($c = 256$).
ResNet-down ($c = 512$).
ResNet-down ($c = 1024$).
ResNet ($c = 1024$).
ReLU. Global pooling. Fully connected (1).

Table 10: Discriminator network architectures for ILSVRC2012 experiments (from [25]). BN stands for batch normalization. c stands for number of channels. k stands for kernel size. s stands for stride.

Direct connection
ReLU. Convolution ($k = 3, s = 1$).
ReLU. Convolution ($k = 3, s = 1$). Average pooling(2).
Shortcut connection
Convolution ($k = 1, s = 1$). Average pooling(2).

Table 11: ResNet-down network architectures for ILSVRC2012 experiments (from [25]). k stands for kernel size. s stands for stride.

Direct connection
Convolution ($k = 3, s = 1$).
ReLU. Convolution ($k = 3, s = 1$). Average pooling(2).
Shortcut connection
Average pooling(2). Convolution ($k = 1, s = 1$).

Table 12: ResNet-first network architectures for ILSVRC2012 experiments (from [25]). k stands for kernel size. s stands for stride.

Direct connection
ReLU. Convolution ($k = 3, s = 1$).
ReLU. Convolution ($k = 3, s = 1$).
Shortcut connection
Convolution ($k = 1, s = 1$).

Table 13: ResNet network architectures for ILSVRC2012 experiments (from [25]). k stands for kernel size. s stands for stride.

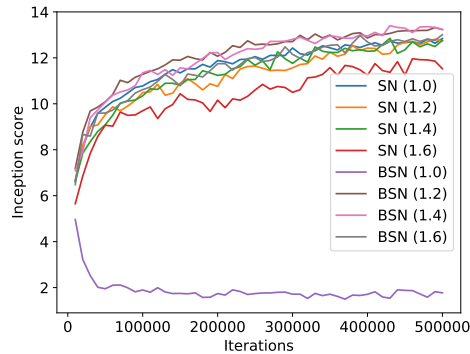


Figure 62: Inception score in ILSVRC2012. The results are averaged over 5 random seeds.

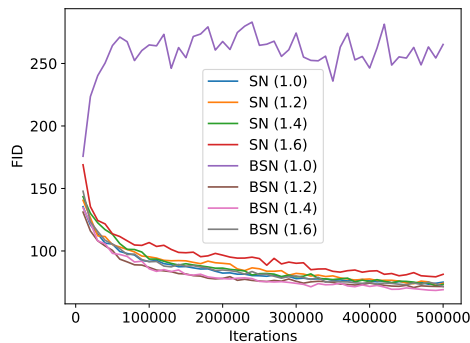


Figure 63: FID in ILSVRC2012. The results are averaged over 5 random seeds.

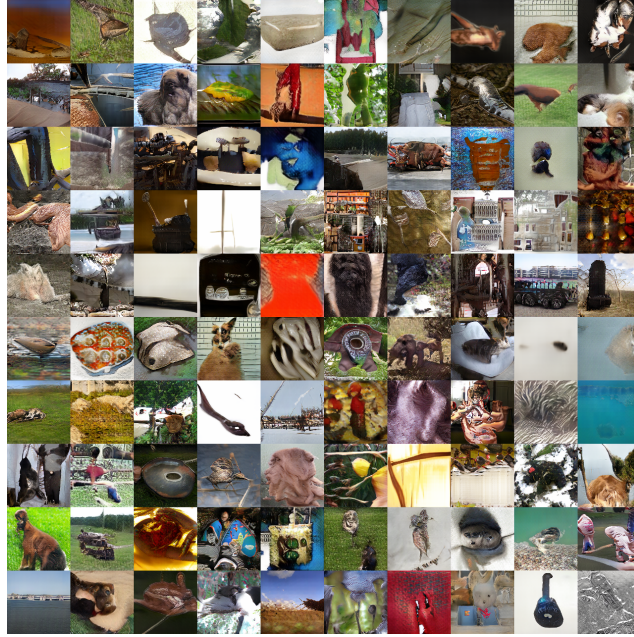


Figure 64: Generated samples from the best run of SN (scale=1.0) in ILSVRC2012. Inception score is 13.50. FID is 72.18.

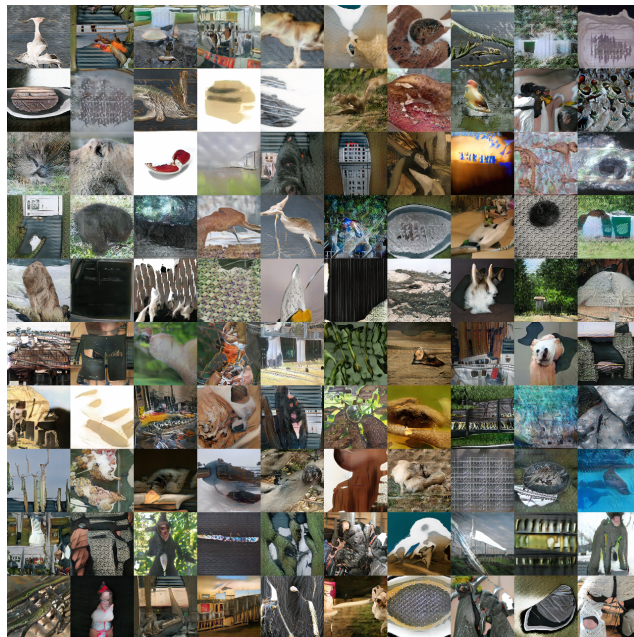


Figure 65: Generated samples from the best run of SN (scale=1.2) in ILSVRC2012. Inception score is 13.04. FID is 72.51.

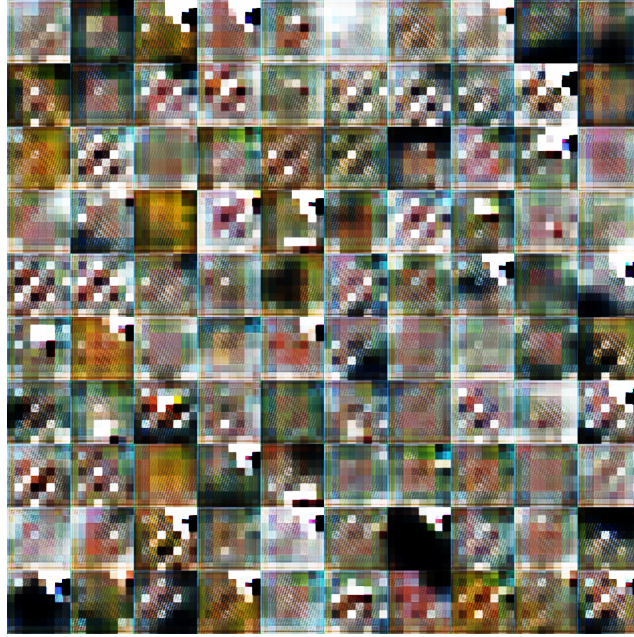


Figure 68: Generated samples from the best run of BSN (scale=1.0) in ILSVRC2012. Inception score is 2.07. FID is 242.51.

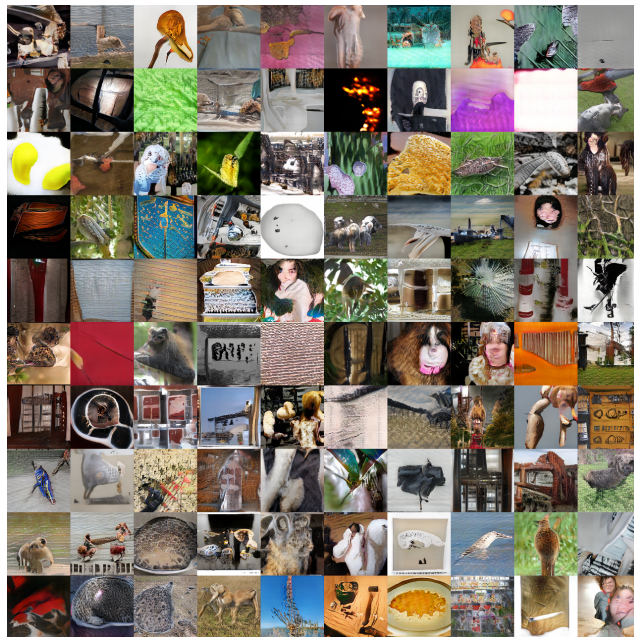


Figure 69: Generated samples from the best run of BSN (scale=1.2) in ILSVRC2012. Inception score is 13.55. FID is 71.30.

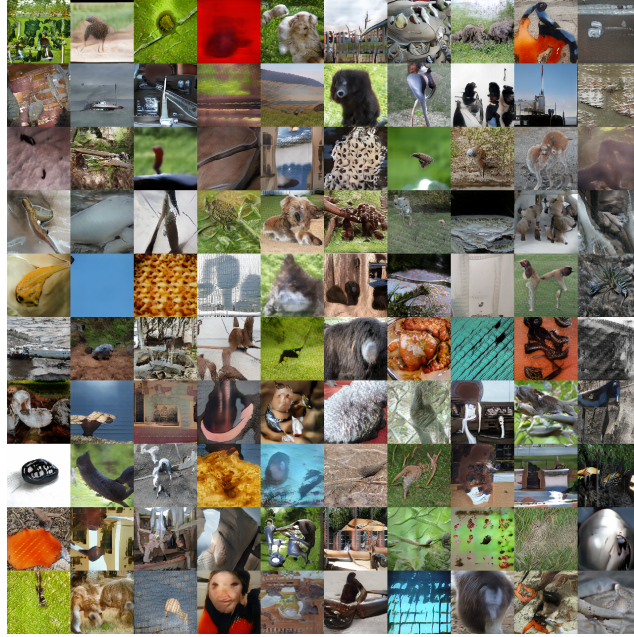


Figure 70: Generated samples from the best run of BSN (scale=1.4) in ILSVRC2012. Inception score is 13.63. FID is 70.88.

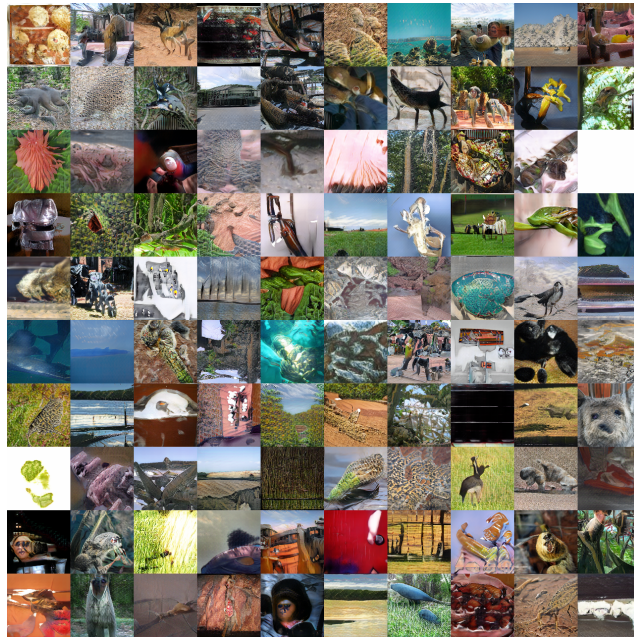


Figure 71: Generated samples from the best run of BSN (scale=1.6) in ILSVRC2012. Inception score is 13.24. FID is 69.06.